

The DeCAMFounder: Non-Linear Causal Discovery in the Presence of Hidden Variables

Raj Agrawal[†]

Laboratory for Information & Decision Systems, Massachusetts Institute of Technology, Cambridge, USA

Chandler Squires

Laboratory for Information & Decision Systems, Massachusetts Institute of Technology, Cambridge, USA.

Neha Prasad

Laboratory for Information & Decision Systems, Massachusetts Institute of Technology, Cambridge, USA.

Caroline Uhler

Laboratory for Information & Decision Systems, Massachusetts Institute of Technology, Cambridge, USA.

Abstract. Many real-world decision-making tasks require learning causal relationships between a set of variables. Typical causal discovery methods, however, require that all variables are observed, which might not be realistic in practice. Unfortunately, in the presence of latent confounding, recovering causal relationships from observational data without making additional assumptions is an ill-posed problem. Fortunately, in practice, additional structure among the confounders can be expected, one such example being *pervasive confounding*, which has been exploited for consistent causal estimation in the special case of linear causal models. In this paper, we provide a proof and method to estimate causal relationships in the non-linear, pervasive confounding setting. The heart of our procedure relies on the ability to estimate the pervasive confounding variation through a simple spectral decomposition of the observed data matrix. We derive a DAG score function based on this insight, and empirically compare our method to existing procedures. We show improved performance on both simulated and real datasets by explicitly accounting for both confounders and non-linear effects.

Keywords: Causal additive models; Graphical models; Non-linear causal discovery; Pervasive confounding; Spectral deconfounding.

1. Introduction

Many decision-making and scientific tasks require learning causal relationships between observed variables. For example, biologists seek to identify causal pathways in gene-regulatory networks, epidemiologists search for the causes of diseases in complex social

[†]*Address for correspondence:* Raj Agrawal, Massachusetts Institute of Technology, Cambridge, MA, United States of America. Email: r.agrawal@csail.mit.edu.

networks, and data scientists in large companies or government agencies vet the biases of their machine-learning models by investigating their causal structure (Spirtes et al., 2000; Friedman et al., 2000; Pearl, 2009; Robins et al., 2000; Kusner et al., 2017). While linear causal methods are often used to model such relationships, they can fail to learn more nuanced information from the data. For instance, in time series data, some variables may exhibit seasonal variation, so that their dependence on time varies sinusoidally. In other instances, variables may exhibit non-monotonic (e.g., quadratic) dependence on their causes; an individual’s health, for example, may generally be an increasing function of the amount of exercise they do, but may begin to decline with over-exercise. In either case, such trends have weak linear correlation. Hence, a linear causal model may lead to poor estimates of the DAG.

To remedy the limitations of linear methods, recent advancements in causal structure discovery have focused on recovery in the *nonlinear causal additive setting*, which assumes that each variable equals a nonlinear function of its parents plus independent noise (Hoyer et al., 2009; Mooij et al., 2009; Peters et al., 2014; Bühlmann et al., 2014). While these non-linear methods consistently recover the true DAG, they assume that all variables are measured, i.e., no latent confounding. However, in many real-world applications, we might expect missing variables. For example, in the social sciences (e.g., economics or psychology), it can be tricky or impossible to measure potential confounders (e.g., abstract variables such as “the market”, “happiness”, etc.). Unfortunately, in the presence of such confounding, a DAG can no longer accurately capture the dependencies among the random variables (Richardson and Spirtes, 2002).

In the seminal work by Richardson and Spirtes (2002), the authors introduced a larger family of graphical models called *ancestral graphs* to account for confounding. While this work considers arbitrary patterns of confounding, we sometimes expect more structure about the confounders in real-world systems. For example, in gene-expression data, batch effects can lead to incorrect associations between genes (Leek and Storey, 2007). In genome-wide association studies, ancestry differences between case and controls can create spurious correlations in disease studies (Price et al., 2006). In finance, latent “market” and “sector” variables can explain much of the variation in stocks (Chandrasekaran et al., 2012; Fan et al., 2013). Such confounders that have an effect on many observed variables are known as *pervasive confounders*; see Frot et al. (2019); Wang and Blei (2019); Shah et al. (2020); Chandrasekaran et al. (2012) for other real-world examples with pervasive confounders. Under the assumption that the confounders are pervasive, Frot et al. (2019); Shah et al. (2020) show how to recover the true causal structure over the observed variables, i.e., the DAG corresponding to the conditional distribution of the observed variables, given the confounders. However, they both assume that all causal relationships are *linear*.

Contributions. In this paper, we consider causal discovery in the non-linear additive noise and pervasive confounding setting. We show that the true graph is still recoverable in Theorem 1 and we provide a practical method for estimation in Section 4.3. The heart of our procedure relies on the ability to estimate the pervasive confounding variation through a simple spectral decomposition of the observed data matrix using a principal components analysis. This approach is similar in spirit to the *Deconfounder* algorithm

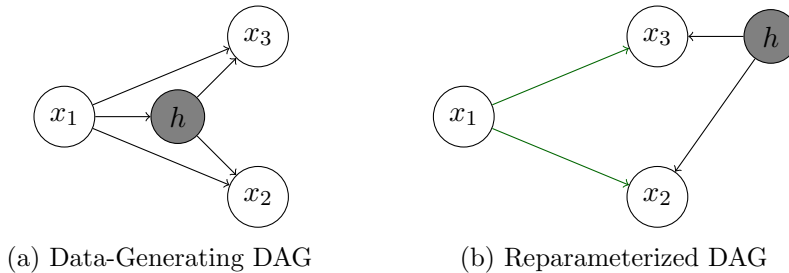


Figure 1: The right hand figure reparameterizes the model on the left such that the unobserved variable (i.e., shaded node) is a source in the graph. The green arrows represent the DAG corresponding to the conditional distribution $\mathbb{P}(x | h)$.

proposed by Wang and Blei (2019), where the goal is not structure discovery but rather estimating average treatment effects.

Outline. The remainder of the paper is structured as follows: we start in Section 2 by formalizing the target of inference and the assumptions about the data generating process. In Section 3, we discuss related methods for causal discovery in the presence of confounders. We conclude by comparing our method, which we outline in Section 4, to existing methods on both real and synthetic datasets in Section 5.

2. Problem Statement: Causal Discovery in the Presence of Confounding

Preliminaries. We would like to estimate the causal relationships between the components of $x \in \mathbb{R}^p$ given N observational datapoints $\{x^{(n)}\}_{n=1}^N$, where $x^{(n)} \stackrel{\text{iid}}{\sim} \mathbb{P}(x)$. Since we assume the existence of unmeasured confounders, in general there does not exist a DAG G such that $\mathbb{P}(x)$ factorizes as $\prod_{i=1}^p \mathbb{P}(x_i | \text{Pa}_G(x_i))$, where $\text{Pa}_G(x_i)$ denotes the parents of x_i in G (Richardson and Spirtes, 2002). Problematically, this factorization or *Markov* property is required by many existing causal learning algorithms to correctly recover causal relationships; see, for example, Chickering (2002); Kalisch and Bühlmann (2007); Solus et al. (2020); Peters et al. (2014). Instead, we might imagine a true underlying data-generating process $(x, h) \in \mathbb{R}^{p+K}$ such that $\mathbb{P}(x, h)$ indeed factorizes according to a DAG G^* , where h plays the role of the latent confounders. Then, the resulting *structural causal model* (SCM) associated with G^* implies that each variable x_j can be written as a function f_j of its parents in G^* and independent noise ϵ_j . Hence, a directed edge $x_i \rightarrow x_j$ in the graph represents that x_i is a direct cause of x_j .

In general, the dependencies between h and x can be complex. For example, if $x_1 = \text{age}$, $x_2 = \text{education}$, $x_3 = \text{health}$, $h = \text{income}$, we might expect that h is a cause of both x_2 and x_3 , and a child of x_1 ; see also Fig. 1a. However, we prove in Proposition 1 that we can always reparameterize the model to remove some of these complex dependencies. In particular, we can construct new latent confounders that are exogenous (i.e., sources in the graph) without modifying the causal ordering of the observed variables.

Proposition 1. *Suppose that the joint distribution \mathbb{P} of a random vector $(x, h) \in \mathbb{R}^{p+K}$ is Markov with respect to a causal DAG G . Then, there exists an exogenous $h' \in \mathbb{R}^K$*

and joint distribution \mathbb{P}' and DAG G' , such that (1) $\mathbb{P}'(x, h')$ is Markov with respect to G' , (2), $\mathbb{P}(x) = \mathbb{P}'(x)$, and (3) the partial order induced by G' equals the partial order induced by G on the subset of observed nodes $\{x_1, \dots, x_p\}$.

We prove Proposition 1 in Appendix A. The main proof idea is taking the structural causal model for (x, h) , and letting h' equal the independent noise terms in h . In light of Proposition 1, we assume throughout that the latent confounders $h \in \mathbb{R}^K$ are sources, i.e., have no observed variables as parents. Hence, conditional on the confounders, $\mathbb{P}(x | h)$ also factorizes according to a DAG, namely the one formed by removing h and all arrows pointing out of h from the full DAG over (x, h) (i.e., the green arrows in Fig. 1b).

Target of Inference. In this paper, we would like to recover G^* , the DAG associated with the conditional distribution $\mathbb{P}(x | h)$ using only the N observed datapoints $\{x^{(n)}\}_{n=1}^N$. Since h is exogenous, the SCM simplifies to

$$x_j = f_j(x_{\text{Pa}_{G^*}(j)}, h, \epsilon_j),$$

where $h \sim \prod_{k=1}^K \mathbb{P}(h_k)$, $\epsilon \sim \prod_{i=1}^p \mathbb{P}(\epsilon_i)$, $h \perp\!\!\!\perp \epsilon$. Unfortunately, due to the curse of dimensionality, the number of datapoints required to accurately estimate f_j depends exponentially on the number of parents (Gyorfi et al., 2003). Given this statistical hardness result, we assume that each f_j has low-dimensional structure.

Causal additive models (CAMs) are a popular way of introducing low-dimensional structure to strike the balance between flexibility and statistical efficiency (Bühlmann et al., 2014). A CAM assumes that each node can be written as an additive function of its parents and independent noise. We make this assumption and consider the following model in this paper:

$$\begin{aligned} x_j &= \sum_{x_i \in \text{Pa}_{G^*}(x_j)} f_{ij}(x_i) + \sum_{k=1}^K g_{kj}(h_k) + \epsilon_j \\ &= \sum_{x_i \in \text{Pa}_{G^*}(x_j)} f_{ij}(x_i) + d_j + \epsilon_j, \quad \text{where} \quad d_j = \sum_{k=1}^K g_{kj}(h_k), \end{aligned} \tag{1}$$

where the f_{ij} and g_{kj} are unknown functions. If we define a new noise term $\tilde{\epsilon}_j = d_j + \epsilon_j$, then this model is equivalent to an SCM with correlated errors.

Problem Statement. If we could remove the direct confounding effect d_j on each node x_j , then $x_j - d_j$ factorizes according to G^* . Hence, applying the procedures developed in Peters et al. (2014); Bühlmann et al. (2014) on the data $\{x_j^{(n)} - d_j^{(n)}\}_{n=1}^N$ recovers G^* as $N \rightarrow \infty$. Of course, the whole discussion so far and the motivation of our paper is that h is not observed. Hence, we cannot directly use existing non-linear causal discovery methods to recover G^* . The main two results of this paper (Theorem 1 and Theorem 2) show that when h has an effect on many variables, then we can construct “sufficient statistics” s_1, \dots, s_p of h using a principal component analysis (PCA) on the observed data. In particular, we show how to construct $s = (s_1, \dots, s_p)$ and show that $\mathbb{P}(x | s)$ factorizes according to G^* .

Before presenting our method in Section 4, we first discuss related methods for learning causal structure in the presence of confounding.

3. Existing Causal Discovery Methods

Two approaches for learning causal structure in the presence of confounders have been proposed. The first approach models the conditional independence structure of $\mathbb{P}(x)$ using an ancestral graph and then tries to recover edges in this graph. Algorithms for this include *FCI* (Spirtes et al., 2000), *RFCI* (Colombo et al., 2012), and *GSPo* (Bernstein et al., 2020). Apart from the computational intensiveness of some of these algorithms, the price of not assuming any structure about the confounders translates into weaker identifiability results relative to methods that exploit additional structural assumptions; see, for example, Figure 1 of (Frot et al., 2019).

The second approach assumes special structure about the confounders, namely that the confounders have an effect on a non-vanishing proportion of the observed variables as $p \rightarrow \infty$. Such variables are called *pervasive confounders*.

Definition 1. h_k is a *pervasive confounder* if $\text{Ch}_{G^*}(h_k) \rightarrow \infty$ as $p \rightarrow \infty$, where $\text{Ch}_{G^*}(h_k)$ denotes the children of h_k in G^* .

This type of confounding structure has been exploited for matrix completion and high-dimensional covariance estimation tasks (Cai et al., 2010; Chandrasekaran et al., 2009; Fan et al., 2013). More recently, similar ideas have been used for learning both directed and undirected Gaussian graphical models. Directed Gaussian graphical models are a special case of the SCM in Eq. (1) considered in this paper, namely where f_{ij} and g_{ij} are linear and ϵ_j is Gaussian; in this case, Eq. (1) simplifies to the more familiar form:

$$x = Bx + \Theta h + \epsilon \quad \text{s.t.} \quad \epsilon \sim N(0, D), \quad h \sim N(0, I),$$

where $B \in \mathbb{R}^{p \times p}$ and $\Theta \in \mathbb{R}^{p \times K}$ are upper-triangular matrices consisting of edge weights. Hence,

$$x = (I - B)^{-1}\epsilon + (I - B)^{-1}\Theta h. \quad (2)$$

In the Gaussian setting with pervasive confounders, a number of methods have been proposed to consistently estimate the covariance matrix of the conditional distribution $\mathbb{P}(x | h)$ using only datapoints drawn from $\mathbb{P}(x)$ (Chandrasekaran et al., 2012; Fan et al., 2013; Frot et al., 2019; Shah et al., 2020). Since in this setting the covariance matrix suffices for conditional independence testing, these methods can consistently recover the true graph up to its Markov equivalence class for directed Gaussian graphical models. The methods for estimating the underlying covariance matrix in the Gaussian setting fall into two approaches, which we call the *spectral approach* and the *optimization approach* and which we describe below. Our proposed method generalizes the spectral approach.

Optimization Approach: Deconfounding the Precision Matrix. This approach starts by decomposing the precision matrix of (x, h) into the blocks

$$[\text{Cov}((x, h))]^{-1} = \begin{pmatrix} J_O & | & J_{OH} \\ \hline J_{HO} & | & J_H \end{pmatrix}.$$

By standard theory for multivariate Gaussian distributions, $J_O \in \mathbb{R}^{p \times p}$ is the precision matrix of the conditional distribution $\mathbb{P}(x | h)$, and hence the target of inference. The key idea for estimating J_O is to relate the observed precision matrix $[\text{Cov}(x)]^{-1}$ and the target quantity J_O via Schur complements:

$$[\text{Cov}(x)]^{-1} = J_O - J_{OH}J_{HH}^{-1}J_{HO}.$$

For sparse DAGs, J_O is a sparse matrix, and for $K \ll p$, $J_{OH}J_{HH}^{-1}J_{HO}$ is low-rank. Hence, when the confounders are pervasive, it is possible to estimate each component through a low-rank plus sparse matrix decomposition of $[\text{Cov}(x)]^{-1}$ (Chandrasekaran et al., 2009; Chandrasekaran et al., 2012).

Spectral Approach: Deconfounding the Covariance Matrix. In contrast to the optimization approach, this approach works towards an estimate of the covariance matrix. Using the SCM in Eq. (2), we obtain

$$\begin{aligned} \text{Cov}(x) &= (I - B)^{-1}D(I - B)^{-T} + (I - B)^{-1}\Theta\Theta^T(I - B)^{-T} \\ &= (I - B)^{-1}D(I - B)^{-T} + \tilde{\Theta}\tilde{\Theta}^T \quad \text{s.t.} \quad \tilde{\Theta} = (I - B)^{-1}\Theta \\ &= \underbrace{J_O^{-1}}_{\text{sparse inverse}} + \underbrace{\tilde{\Theta}\tilde{\Theta}^T}_{\text{low-rank}}. \end{aligned} \quad (3)$$

If the confounders are pervasive, then a non-negligible fraction of Θ is non-vanishing and the eigenvalues of $\tilde{\Theta}\tilde{\Theta}^T$ grow linearly with the dimension p . However, the eigenvalues of J_O are bounded. As a result, the spectrum of $\text{Cov}(x)$ is dominated by the spectrum of $\tilde{\Theta}\tilde{\Theta}^T$ if its eigenvalues diverge significantly from those of J_O , i.e. they are well-separated. Hence, the first K principal components of $\text{Cov}(x)$ approximate $\tilde{\Theta}\tilde{\Theta}^T$ well, and consequently provide a way to separate out J_O^{-1} (Fan et al., 2013; Wang and Fan, 2017). In settings when the eigenvalues of J_O^{-1} and $\tilde{\Theta}\tilde{\Theta}^T$ in Eq. (3) are not well-separated, Shah et al. (2020) propose a modified covariance estimator and use it for learning the causal model in the linear setting. Outside of the graphical models literature, the spectral approach is also similar in flavor to the approach proposed by Wang and Blei (2019) to estimate average treatment effects in the potential outcomes framework.

The current methods described above for learning in the presence of pervasive confounders are all grounded in the linear setting. In the next section, we show how to extend these techniques to the nonlinear causal additive setting. As we will see, current methods are *not* consistent in this setting, and need careful modification. In particular, the methods above only estimate the low-rank component for the purpose of removing it, creating a new “processed” version of the data. However, in the nonlinear causal additive setting, the low-rank component plays a more complex role, as we now show.

4. Our Method

Our goal is to learn G^* , the DAG induced by the conditional distribution $\mathbb{P}(x | h)$ under the model in Eq. (1). In Section 4.1, we introduce a sufficient statistic s of the confounders h , and prove that $\mathbb{P}(x | s)$ also factorizes according to G^* . It therefore suffices to estimate

s in order to recover G^* . In Section 4.2 we show that in the pervasive confounding setting, we can consistently estimate s using a principal components analysis on the observed data. We conclude in Section 4.3 by proposing a new score function that scores DAGs using these estimates of s .

In what follows, we assume without any loss of generality that $\pi^* := (1 \cdots p)$ is a consistent topological ordering of G^* (i.e., that x_i can only be a cause not an effect of a variable x_j when $i < j$) to simplify notation.

4.1. Sufficient Statistics for Recovering the DAG

Our main theorem below, which we prove in Appendix A, says that $\mathbb{P}(x | s)$ factorizes according to G^* when s equals the conditional expectation $\mathbb{E}[x | h]$.

Theorem 1. *There exist functions $\{r_j\}_{j=1}^p$ such that the SCM in Eq. (1) can be re-written as*

$$x_j = \sum_{x_i \in Pa_{G^*}(x_j)} f_{ij}(x_i) + [s_j - r_j(s_1, \dots, s_{j-1})] + \epsilon_j,$$

where

$$s_j = \mathbb{E}[x_j | h].$$

Hence, the conditional distribution $x | s$ factorizes according to G^* .

Corollary 1. *G^* is identifiable from the conditional distribution $x | s$ when all the f_{ij} are non-linear and three-times differentiable.*

Proof. By Theorem 1, $x | s$ factorizes according to G^* . Since $\epsilon_j \perp\!\!\!\perp \{(x_i, r_i)\}_{i=1}^{j-1}$, the SCM in Theorem 1 is an additive noise model. By Corollary 31 of Peters et al. (2014), G^* is identifiable from observational data alone. \square

By Corollary 1, the task of identifying G^* reduces to one of computing or estimating s . Since we do not know h , we cannot estimate s by regressing x on h . Before showing how we can implicitly estimate s using principal components analysis in the next section, we describe the special linear case to build intuition for Theorem 1.

Example 1. In the linear setting of Eq. (2),

$$\begin{aligned} s &= \mathbb{E}[x | h] \\ &= \mathbb{E}[(I - B)^{-1}\epsilon + (I - B)^{-1}\Theta h | h] \\ &= (I - B)^{-1}\Theta h, \quad \text{since } \epsilon \perp\!\!\!\perp h \text{ and } \mathbb{E}[\epsilon] = 0. \end{aligned}$$

Lemma 1 below, which we prove in Appendix A using a simple recursive argument, allows us to re-write each entry s_j of s in a more revealing form.

Lemma 1. *In the linear setting,*

$$\begin{aligned} s_j &= [(I - B)^{-1}\Theta h]_j \\ &= \sum_{i \in Pa_{G^*}(x_j)} B_{ij}[(I - B)^{-1}\Theta h]_i + \Theta_{j,\cdot}^T h, \end{aligned}$$

where $\Theta_{j,\cdot}$ denotes the j th row of Θ .

Recalling that $d_j = \Theta_{j,\cdot}^T h = s_j - r_j$, then

$$\begin{aligned} r_j &= \sum_{i \in \text{Pa}_{G^*}(x_j)} B_{ij} [(I - B)^{-1} \Theta h]_i. \\ &= \sum_{i \in \text{Pa}_{G^*}(x_j)} B_{ij} s_i \quad (\text{by Lemma 1}). \end{aligned} \tag{4}$$

Therefore, the SCM in Eq. (2) can be re-written as

$$(x_j - s_j) = \sum_{x_i \in \text{Pa}_{G^*}(x_j)} B_{ij} (x_i - s_i). \tag{5}$$

If we can estimate s_j , then Eq. (5) leads to a natural data pre-processing algorithm: given an input dataset $\{x^{(n)}\}_{n=1}^N$, provide the analyst with the processed dataset $\{(x^{(n)} - s^{(n)})\}_{n=1}^N$. Given this processed dataset, the analyst can then feed this data into a linear causal learning algorithm and learn G^* up to its Markov equivalence class.

In the next section, we provide settings under which s can be estimated consistently in the non-linear setting and also provide statistical rates of convergence for our estimator.

4.2. Asymptotically Exact Estimates of the Sufficient Statistics

To estimate s , we reduce our problem into the linear latent factor setting studied by Fan et al. (2013); see also Section 3.

Reduction to Fan et al. (2013). Let μ^* denote the joint distribution of (ϵ, h) . Assume that each random variable $x_j \in \mathcal{H}^* \subset \mathbb{L}^2(\mu^*)$, where \mathcal{H}^* is a complete Hilbert space and $\mathbb{L}^2(\mu^*)$ consists of all square-integrable functions of (ϵ, h) with respect to the measure μ^* . Then, there exists M (possibly equal to infinity) set of basis functions $\{\phi_m\}_{m=1}^M$ such that

$$\begin{aligned} s_j &= \mathbb{E}[x_j | h] \in \mathcal{H}_M := \text{span}\{\phi_1(h), \dots, \phi_M(h)\} \quad \forall j \in [p] \\ &= \psi_j^T \Phi(h), \quad \Phi(h) := [\phi_1(h), \dots, \phi_M(h)]^T, \end{aligned}$$

since \mathcal{H}^* is separable (Rudin, 1974).

Assumption 1. Suppose there exists $M < \infty$ such that $s_j \in \mathcal{H}_M$ for all $j \in [p]$.

Under Assumption 1, we can express the n th datapoint $(x^{(n)}, h^{(n)}) \stackrel{\text{iid}}{\sim} \mathbb{P}(x, h)$ as

$$\begin{aligned} x^{(n)} &= \mathbb{E}[x^{(n)} | h^{(n)}] + [x^{(n)} - \mathbb{E}[x | h^{(n)}]] \\ &= \Psi \Phi(h^{(n)}) + u^{(n)}, \quad u^{(n)} := x^{(n)} - \Psi \Phi(h^{(n)}), \end{aligned} \tag{6}$$

where the j th row is $\Psi_{j,\cdot} = \psi_j^T$. Since $u^{(n)}$ is simply the residual after removing all of the variation explained by h , it holds that $\text{Cov}(\Phi(h), u) = 0_{M \times p}$. Hence, $\Phi(h^{(n)})$, which plays the role of the *latent factors* in Fan et al. (2013), and $u^{(n)}$ are uncorrelated. Then, the model in Eq. (6) is equivalent to the one studied by Fan et al. (2013).

Our estimator for $s^{(n)} = \Psi\Phi(h^{(n)})$ below is mathematically equivalent to the least-squares estimator provided in Section 2.3 of Fan et al. (2013). Although our estimator is equivalent, we derive the estimator from the perspective of matrix perturbation theory instead of least-squares. This alternative formulation provides additional geometric insights.

Derivation of the Estimator. By Eq. (6), we can decompose the data matrix $X \in \mathbb{R}^{N \times p}$ as,

$$\begin{aligned} X = S + U \quad \text{s.t.} \quad X &= [x^{(1)} \dots x^{(N)}]^T, \quad S = [s^{(1)} \dots s^{(N)}]^T, \\ U &= [u^{(1)} \dots u^{(N)}]^T. \end{aligned}$$

The goal is to deconvolve S from the observable X . U can be viewed as playing the role of a perturbation to the matrix of interest S . To apply matrix perturbation results such as Weyl’s eigenvalue theorem and the $\sin(\theta)$ theorem (Davis and Kahan, 1970), we need to understand the spectral properties of S and U . To this end, if $M < \max(N, p)$, then S has rank M . Hence,

$$\begin{aligned} \|S\|_F^2 &= \sum_{m=1}^p \lambda_m(S^T S) \\ &= \sum_{m=1}^M \lambda_m(S^T S), \quad (\text{since } \lambda_m(S^T S) = 0 \text{ for } m > M), \end{aligned} \tag{7}$$

where $\lambda_m(\cdot)$ denotes the m th largest eigenvalue of a matrix. If h has an effect on many variables, or equivalently if Ψ has many non-zero entries, then $\|S\|_F^2 \rightarrow \infty$. By Eq. (7), this implies that the top M non-zero eigenvalues of S must also go to infinity. Therefore, the spectrum of S is concentrated or *spiked* on M eigenvalues instead of being spread out on all p possible eigenvalues. Conversely, for sparse G^* with bounded node degrees, the eigenvalues of U are diffuse and bounded. Intuitively, the eigenvalues are not large because there are no “directions” that capture much of the variability or variance in U due to the sparsity condition on G^* . This discrepancy between the spectra of S and U give rise to a natural estimator to recover S : project X onto an M -dimensional subspace using principal component analysis (PCA). Since most of the variability in X occurs in the subspace spanned by S , PCA should output a subspace close to S . Recalling the many equivalent characterizations of PCA, we can find this projection by solving for the one that minimizes the empirical squared reconstruction loss:

$$\begin{aligned} \Pi_{\text{PCA}}^* &= \arg \min_{\text{rank}(\Pi) \leq M} \frac{1}{N} \sum_{n=1}^N \|x^{(n)} - \Pi(x^{(n)})\|_2^2. \\ &= \arg \min_{\text{rank}(\Pi) \leq M} \|X - \Pi(X)\|_2^2 \quad \text{s.t.} \quad \Pi(X) = [\Pi(x^{(1)}) \dots \Pi(x^{(N)})]^T \\ &= \arg \min_{\text{rank}(\Pi) \leq M} \|X - \Pi(X)\|_F^2. \end{aligned}$$

Fortunately, this optimization problem has a closed-form solution, namely

$$\Pi_{\text{PCA}}^*(x) = V_M V_M^T x \quad \text{s.t.} \quad \hat{\Sigma} = V \Lambda V^T, \tag{8}$$

where $\hat{\Sigma}$ is the sample covariance matrix, $V\Lambda V^T$ is the eigendecomposition of $\hat{\Sigma}$, and V_M is the matrix consisting of the top M eigenvectors of V . Then, our estimate $\hat{s}_j^{(n)}$ of $s_j^{(n)} = [S]_{nj}$ equals

$$\hat{s}^{(n)} = \Pi_{\text{PCA}}^*(x^{(n)}) = V_M V_M^T x^{(n)}.$$

Theorem 2. *Under Assumption (1)-(4) of Fan et al. (2013), and Assumption 1,*

$$\max_{1 \leq j \leq p, 1 \leq n \leq N} \|\hat{s}_j^{(n)} - s_j^{(n)}\|_2 = O_p \left(\log(N)^{1/c} \sqrt{\frac{\log p}{N}} + \frac{N^{\frac{1}{4}}}{\sqrt{p}} \right),$$

for some constant $c > 0$.

Proof. See Corollary 1 of Fan et al. (2013). \square

Hence, ignoring log factors, we can estimate $s_j^{(n)}$ at the rate $\tilde{O} \left(\frac{1}{\sqrt{N}} + \frac{N^{\frac{1}{4}}}{\sqrt{p}} \right)$. Therefore, we need both p and N to grow for consistent estimation of $s_j^{(n)}$. Intuitively, as p grows, the eigenvalues or “spikiness” of S increases, making the projection via PCA tend towards S ; for a precise statement, see Proposition 1 and 2 of Fan et al. (2013). On the other hand, as N grows, the estimate of the covariance matrix improves and thereby reduces the estimation error of projecting via the sample covariance matrix. In the original paper by Fan et al. (2013), the authors required that $\Phi(h)$ have an effect on $O(p)$ variables. In later work by Wang and Fan (2017), the authors showed that this dependence can be weakened to $O(\sqrt{p})$; see Theorems 3.1 and 3.2 of Wang and Fan (2017).

Algorithm 1 summarizes our approach for estimating the matrix of sufficient statistics S . In practice, we might not know what M to use in Algorithm 1. To this end, we can use the estimator provided in Section 2.4 of Fan et al. (2013) to estimate M . As we show in Section 5, it is often easier to instead visually inspect the spectrum of the sample covariance matrix (i.e., the scree plot) to pick M .

4.3. The DeCAMFounder Score Function

In this section, we exploit the special conditional independence structure implied by Theorem 1 as well as Algorithm 1 to estimate G^* via a *score-based approach*. In general, score-based approaches consist of two parts: (1) a score-function to measure the quality

Algorithm 1 Principal Confounding Sufficient Statistics

- 1: **procedure** PCSS(X, M)
 - 2: $\hat{\Sigma} = \frac{1}{N} X^T X$
 - 3: $V, \Lambda, V^T = \text{eigen}(\hat{\Sigma})$ ▷ Eigendecomposition of $\hat{\Sigma}$
 - 4: $S = (V_M V_M^T X^T)^T \in \mathbb{R}^{N \times p}$ ▷ Sufficient statistics derived in Eq. (8)
 - 5: **return** S
 - 6: **end procedure**
-

of a DAG and (2) a combinatorial optimization procedure to optimize this score-function over the space of DAGs. There are many existing general-purpose procedures for (2); see, for example, Chickering (2002); Solus et al. (2020); Bühlmann et al. (2014). Hence, we focus our attention on (1), namely developing a score function to estimate the graph in the pervasive confounding setting.

A natural starting point (based on its popularity in the linear setting) might be to use the *Bayesian information criterion* (BIC) as the score function, which penalizes DAGs based on the number of parameters (Chickering, 2002). For linear models, computing this penalty is straightforward because the number of parameters simply equals the number of edges in the graph (corresponding to number of edge weights to be estimated) and p (the number of node noise variances to be estimated). For non-linear models, however, the number of parameters can be infinite. Hence, BIC cannot directly be applied. Instead, we use a Bayesian score, namely the marginal log-likelihood of the DAG (which the BIC approximates with a second-order Taylor series) conditional on the matrix of confounder sufficient statistics S . Specifically, we score a DAG G by

$$\mathbb{P}(X | G, S) = \int_{\Omega_G} \mathbb{P}(X | G, S, \Omega_G) d\mathbb{P}(\Omega_G), \quad (9)$$

where $\mathbb{P}(\Omega_G)$ is a prior over the unknown set of functions $\Omega_G := \{\{f_{ij}\}_{i \in \text{Pa}_G(x_j)}, r_j\}_{j=1}^p$ defining the model (see Theorem 1). In the following, we consider the special setting where the prior $\mathbb{P}(\Omega_G)$ is given by a Gaussian process.

We define our score function, the *DeCAMFounder Score*, by placing Gaussian process priors on Ω_G as in Friedman and Nachman (2000). This choice of prior provides flexibility to model non-linear relationships, while having desirable theoretical properties such as statistical consistency; see, for example, Chapter 7 of Rasmussen and Williams (2006). In the following, we show in Proposition 2 that under suitable assumptions we can analytically compute Eq. (9) by using a GP prior. Based on the analytical formula provided in Proposition 2, we show in Corollary 2 that we can compute Eq. (9) in $O(p\kappa N^2 + pN^3)$ time, where κ depends on the maximum number of parents in G and the functions r_j .

Proposition 2. *Suppose that*

$$\begin{aligned} \epsilon_j &\sim \mathcal{N}(0, \sigma_j^2) \\ f_{ij} &\sim GP(0, k_{\theta_{ij}}(\cdot, \cdot)) \\ r_j &\sim GP(0, k_{\eta_j}(\cdot, \cdot)), \end{aligned}$$

where $k_{\theta_{ij}}(\cdot, \cdot)$ and $k_{\eta_j}(\cdot, \cdot)$ are positive definite kernel functions with kernel hyperparameters θ_{ij} and η_j , and ϵ_j denotes the noise terms in Eq. (1). For all $1 \leq j \leq p$, select $s_{C_j} \subset \{s_1, \dots, s_{j-1}\}$ and a function q_j such that $r_j = q_j(s_{C_j})$ in Theorem 1. Then, Eq. (9) equals

$$\sum_{j=1}^p \log \mathbb{P}(X_j - S_j | X_{\text{Pa}_G(x_j)}, S_{C_j}) = -.5 \sum_{j=1}^p \left[\tilde{X}_j^T L_j^{-1} \tilde{X}_j - \log \det L_j - N \log(2\pi) \right], \quad (10)$$

where $X_j - S_j$, $L_j = K_j + \sigma_j^2 I_{N \times N}$, and $[K_j]_{nm} = k_{\theta_{ij}, \eta_j}((x^{(n)}, s^{(n)}), (x^{(m)}, s^{(m)}))$ for

$$k_{\theta_{ij}, \eta_j}((x, s), (\tilde{x}, \tilde{s})) = \sum_{i \in \text{Pa}_G(x_j)} k_{\theta_{ij}}(x_i, \tilde{x}_i) + k_{\eta_j}(s_{C_j}, \tilde{s}_{C_j}).$$

Corollary 2. *Under the assumptions of Propositions 2, $\mathbb{P}(X | G, S)$ takes $O(p\kappa N^2 + pN^3)$ time to compute, where $\kappa = \max_{1 \leq j \leq p} |\text{Pa}_G(x_j)| + |C_j|$.*

Proof. It suffices to show that $\mathbb{P}(X_j - S_j | X_{\text{Pa}_G(x_j)}, S_{C_j})$ takes $O(\kappa N^2 + N^3)$ time to compute by Proposition 2. k_{θ_{ij}, η_j} takes at most $O(\kappa)$ time to evaluate on a pair of points. Hence, the $N \times N$ kernel matrix K_j takes at most $O(\kappa N^2)$ time to compute. Computing the determinant and inverse of L_j takes $O(N^3)$ time. Finally, the matrix vector multiplication $\tilde{X}_j^T L_j^{-1} \tilde{X}_j$ takes $O(N^2)$ time. \square

We prove Proposition 2 in Appendix A. Since s_{C_j} is not a subset of $s_{\text{Pa}_{x_j}(G)}$ in general, Eq. (10) does not reduce into summands that only depend on the parents in G (i.e., lacks *decomposability*). Decomposability, however, is critical from a computational perspective, since given the marginal likelihood of a DAG G , it allows computing the marginal of a new DAG G' by only recomputing the marginal likelihood of the parent sets that changed relative to G . To this end, we assume, for computational efficiency, that each r_j in Theorem 1 only depends on $s_{\text{Pa}_{G^*}(x_j)}$ in Algorithm 2.

Assumption 2. There exists some q_j such that $r_j = q_j(s_{\text{Pa}_{G^*}(x_j)})$ for all $1 \leq j \leq p$.

Under Assumption 2, we can compute Eq. (9) in $O(p\kappa N^2 + pN^3)$ time, where κ equals two times the maximum number of parents in G by Corollary 2. We might expect that Assumption 2 holds (at least approximately) based on the following considerations: as we show in the proof of Theorem 1 in Appendix A, $r_j = \sum_{i \in \text{Pa}_{G^*}(x_j)} \mathbb{E}[f_{ij}(x_i) | h]$. Since $s_i = E[x_i | h]$, we might expect that there exists a function z_i such that $\mathbb{E}[f_{ij}(x_i) | h] \approx z_i(s_i)$. When f_{ij} is a linear function, for example, then there always exists such a z_i ; see Eq. (4) for the exact formula of z_i . Hence, if $\mathbb{E}[f_{ij}(x_i) | h] \approx z_i(s_i)$, then $r_j \approx \sum_{i \in \text{Pa}_{G^*}(x_j)} z_i(s_i)$ is well approximated by a function of $s_{\text{Pa}_{G^*}(x_j)}$. Under Assumption 2, the log marginal likelihood simplifies into a decomposable score

$$\log \mathbb{P}(X | S, G) = \sum_{j=1}^p \log \mathbb{P}(X_j - S_j | X_{\text{Pa}_G(x_j)}, S_{\text{Pa}_G(x_j)})$$

by Proposition 2. In general, we might not know a priori what kernel hyperparameters θ_{ij}, η_j , or noise variance σ_j to select in Eq. (10).

To this end, we follow the common approach of maximizing the marginal likelihood (also known as Type II maximum likelihood estimation) with respect to these parameters using gradient ascent instead of placing hyperpriors over these parameters (Friedman and Nachman, 2000, Section 4). We summarize our final derived score function in Algorithm 2. In our implementation of the DeCAMFounder score, we use the probabilistic programming language *GPYtorch* (Gardner et al., 2018) to fit kernel hyperparameters via gradient ascent. In Appendix B, we detail the particular kernel functions used in our experiments.

5. Experiments

In this section, we start by empirically assessing how well the *Principal Confounding Sufficient Statistics* or PCSS procedure outlined in Algorithm 1 estimates the confounder sufficient statistics $s = \mathbb{E}[x | h]$. Although PCSS provides asymptotically exact estimates for s by Theorem 2, these estimates are noisy in the finite observational data regime. We test the impact of the estimation error on the performance of our DeCAMFounder score function (which assumes s is provided exactly) for the task of causal discovery in Section 5.1.2 and Section 5.2.2. We benchmark our DeCAMFounder score function against other popularly used score functions in the fully-observed and/or pervasive confounding setting. We discuss these benchmark methods in greater depth in Section 5.1.2.

We start our evaluation with simulated data so as to have access to a known ground truth DAG. In Section 5.2, we then also evaluate our method on an ovarian cancer dataset, which can partially be validated based on prior biological knowledge about the underlying system. We thank the authors in Frot et al. (2019) for providing a pre-processed and easily reproducible version of this dataset (as well as personal assistance). All results can be re-generated using the data and code provided in <https://github.com/uhrerlab/decamfound>.

5.1. Simulated Data

In this set of simulations we analyze the sensitivity and robustness of our method with respect to different data characteristics. To this end, we vary the following parameters: strength of confounding, linear or non-linear SCM, and dimensionality.

Controlling the Strength of Confounding. Generating non-linear (and even linear) data can be challenging. For example, without proper normalization, the variance of downstream nodes will explode (e.g., consider a line graph with edge weights equal to 2). From a signal processing perspective, if the noise variance of each node is drawn from the same distribution (e.g., as in Peters et al. (2014); Hauser and Bühlmann (2012)), then downstream nodes will typically have a higher signal-to-noise ratio than upstream nodes. To prevent such artifacts about the underlying data simulation process to skew results, we use the following normalization (some edge cases occur for source nodes or those independent of h , see Appendix C for details):

Algorithm 2 The DeCAMFounder Score

```

1: procedure DECAM( $X, G, M$ )                                ▷  $G$  a DAG with vertex set  $[p]$ 
2:    $S = \text{PCSS}(X, M)$                                        ▷ Computed from Algorithm 1
3:    $\pi$  is a topological order of  $G$ 
4:    $mll = 0$ 
5:   for  $i$  in  $[p]$  do
6:      $mll = mll + \arg \max_{\theta_{ij}, \eta_j, \sigma_j} [\text{Eq. (10)}]$     ▷ Maximize via gradient ascent
7:   end for
8:   return  $mll$                                              ▷ The log marginal likelihood of  $G$ .
9: end procedure

```

- **Unit variance nodes:** $\text{Var}(x_j) = 1$ for all $j \in [p]$.
- **Zero mean nodes:** $\mathbb{E}[x_j] = 0$ for all $j \in [p]$.
- **Fixed signal, confounding, and noise variances:** for all $j \in [p]$:
 - $\text{Cov}(x_j, \epsilon_j) = \sigma_{\text{noise}}^2$,
 - $\text{Cov}(\sum_{k=1}^K g_{kj}(h_k)) = \sigma_h^2$, and
 - $\text{Cov}(\sum_{x_i \in \text{Pa}_{G^*}(x_j)} f_{ij}(x_i)) = \sigma_{\text{signal}}^2$.

Since all nodes have unit variance, σ_h^2 (σ_{signal}^2) equals the fraction of the variation in x_j explained by h (observed variables), or equivalently, the R^2 of a model where the explanatory variables consist of all confounders (all observed variables). In our experiments, we fix $\sigma_{\text{noise}}^2 = 0.2$. In other words, if we could actually observe both x and h , then the noise in the problem is relatively small. To assess how the strength of confounding affects DAG recovery, we vary σ_h^2 . Note that σ_{signal}^2 is a deterministic function of σ_h^2 : $\sigma_{\text{signal}}^2 = \text{Var}(x_j) - \sigma_{\text{noise}}^2 - \sigma_h^2 = 0.8 - \sigma_h^2$, so that varying σ_h^2 implicitly varies the observed signal variance σ_{signal}^2 .

Linear / Non-Linear SCM. In real data, we often expect certain characteristic patterns such as upward, seasonal, or quadratic trends. Based on this intuition, we draw each f_{ij} and g_{kj} from the set of linear trends $\{\theta x : \theta \in \mathbb{R}^p\}$, seasonal trends $\{\theta \sin(\pi x) : \theta \in \mathbb{R}^p\}$, or quadratic trends $\{\theta x^2 : \theta \in \mathbb{R}^p\}$ when generating non-linear data. For data generated from a linear SCM, we assume that all f_{ij} and g_{kj} belong to the set of linear trends $\{\theta x : \theta \in \mathbb{R}^p\}$.

Data Generation. We randomly draw G^* from an Erdős-Rényi random graph model with expected neighborhood size of 5 and consider graphs with number of observed nodes $p \in \{250, 500, 1000\}$. As in Frot et al. (2019), we assume that each confounder h_k is a direct cause of node x_j with a 70% chance. Given the graph, we randomly select a trend type for each edge (i.e., the f_{ij} and g_{kj}) with equal probability. We then randomly draw a weight $\theta \sim \text{Uniform}([-1, -.25] \cup [.25, 1])$ and appropriately scale weights of all parents simultaneously to satisfy the normalization constraints above. We finally add $N(0, \sigma_{\text{noise}}^2)$ noise to each node; see Appendix C for more details and references to our python code. Unless otherwise stated, we draw 25 random datasets for each specific configuration of confounding strength, dimensionality, etc. We consider $K = 1$ pervasive confounders which allows us to plot how each node varies as a function of this confounder. This confounder could, for example, represent batch effects in biological experiments, the market in stock-market data, or ancestry in genome-wide association studies.

5.1.1. Confounder Sufficient Statistics Estimation Performance

In the following, we quantify the mean-squared estimation error of s . Based on Theorem 2, this error should decrease as N and p increase. To test this empirically, we keep the ratio of $\frac{p}{N}$ fixed at 2 (i.e., the high-dimensional case), and vary the confounding strength,

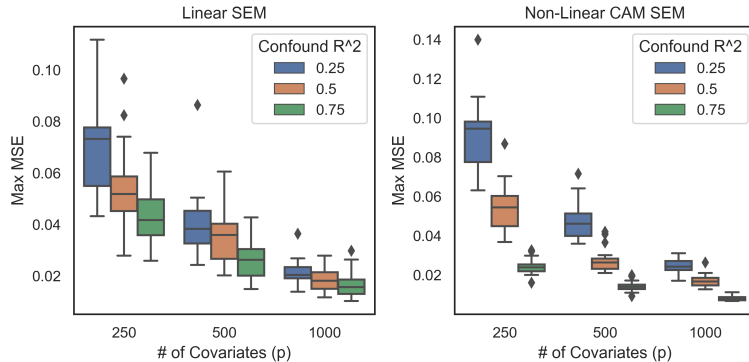


Figure 2: Maximum Mean-Squared Error (MSE) across all dimensions for estimating s via PCSS. Twenty-five total simulations were performed for each dataset configuration.

dimensionality, etc. Fig. 2 shows the maximum mean-squared error which equals

$$\max_{j \in [p]} \frac{1}{N} \sum_{n=1}^N \left(s_j^{(n)} - \hat{s}_j^{(n)} \right)^2.$$

In the linear case, we can compute s analytically (see Lemma 1). In the non-linear case, there is no analytical expression for s . However, for observed nodes x_j that only have confounders as parents, $s_j = \sum_{k=1}^K g_{kj}(h_k) = d_j$. Since we are simulating data and have access to h , we can compute s_j for these nodes. Thus, in Fig. 2, the max MSEs for the non-linear SCM case are only with respect to nodes that have only confounders as parents. From this figure, we see that the MSE decreases as p increases or when the strength of the confounders increases.

To evaluate the quality of PCSS for nodes x_j that occur further downstream (i.e., have some observed nodes as parents), we can make qualitative assessments. In particular, since we only have $K = 1$ confounders, we can plot x_j against h_1 . The visual trend we see from the resulting scatterplot corresponds to the desired conditional expectation $s_j = \mathbb{E}[x_j | h]$. By plotting the confounder sufficient statistics estimated from PCSS on the same plot for each dimension, we can qualitatively check for a matching trend. Fig. 3 shows these scatterplots for a particular random data simulation and select nodes that have at least one parent. We see that PCSS indeed matches the data trend well.

5.1.2. Evaluation of the DeCAMFounder Score

We now transition to evaluating the quality of our DeCAMFounder score function, which depends on noisy estimates of s via PCSS to score DAGs. For this, we want to separate the merits of the score function from the underlying combinatorial optimization procedure. Since most score functions used in practice are decomposable (including ours), we can reduce the evaluation to the task of effectively scoring parent sets; typical DAG optimization procedures build up a DAG by greedily optimizing over parent sets (Chickering, 2002). As we show below, this reduction not only allows us to abstract

out the challenging combinatorial optimization problem but also enables us to evaluate methods on larger scale datasets since we do not need to score the whole DAG. Our method, similar to existing kernel constraint-based methods such as RESIT (Peters et al., 2014), takes $O(N^3)$ time to score a single parent set.

Description of the Parent Set Evaluation Tasks. A local change to a parent set in greedy procedures typically involves a single node addition (i.e., adding a node to the current parent set) or deletion (i.e., removing a node from the current parent set). In the presence of latent confounding, methods that do not account for confounders are susceptible to adding spurious edges. For example, if nodes x_i and x_j have a common cause, a method that assumes no latent confounding might add an edge from x_i to x_j or vice versa with high probability, even when all the true parents of the node are *included* in the current parent set. This observation leads to a natural evaluation procedure: consider the set of all nodes $C := \{x_j : d_j \neq 0\}$ that have a direct confounding effect. Randomly select a node $x_{j'}$ from C and randomly sample M nodes x_{r_1}, \dots, x_{r_M} from C that are not parents of $x_{j'}$. Then, we can evaluate the methods in terms of scoring the following $M + 1$ parent sets:

$$P_{\text{correct}} = \text{Pa}_{G^*}(x_{j'})$$

$$P_i = \text{Pa}_{G^*}(x_{j'}) \cup \{x_{r_i}\} \quad \text{for } i \in [M].$$

Again, we might expect that methods that do not correct for confounders score the P_i higher than P_{correct} due to spurious correlations created by the confounders. In our evaluation, we pick $M = 100$. We call this evaluation procedure the *Wrong Parent Addition Task*. We note that this task is similar to the popular ‘‘CauseEffectPairs’’ causality challenge introduced by Mooij et al. (2016).

The second parent set evaluation task concerns the node deletion phase. Here, we expect that linear methods may suffer by potentially removing true parent nodes. For example, if a parent node has weak *linear* correlation with the target node (e.g., as is the case with our sine and quadratic trends), then that parent would likely be pruned off using a sparsity-inducing score function such as BIC or penalized log-likelihood with an L_0 or L_1 penalty.

Similar to the Wrong Parent Addition task, we first randomly select a node $x_{j'}$ with

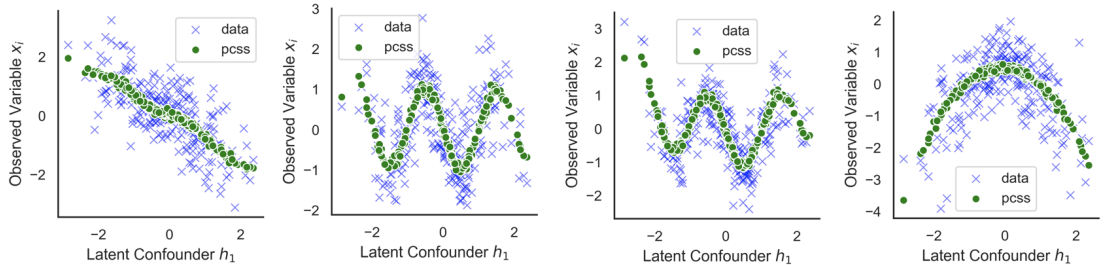


Figure 3: Non-linear estimation of $E[x_i | h]$ via PCSS for nodes with at least one parent.

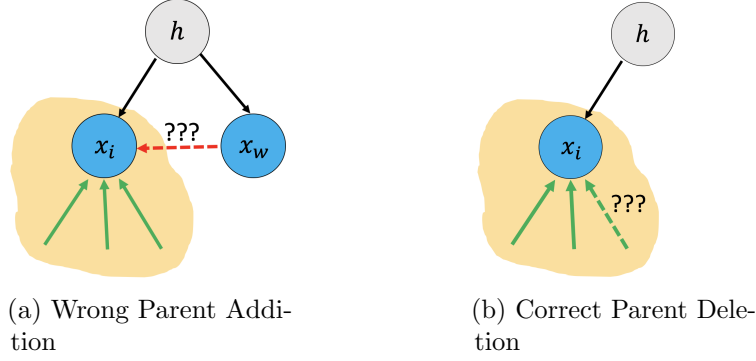


Figure 4: Our parent set evaluation tasks. Green arrows represent the set of true edges, and red arrows indicate incorrect edges. Dotted arrows indicate a potential incorrect modification to the true parent set of a node.

at least one observed parent node. For each node in the parent set of $x_{j'}$, let

$$P_{\text{correct}} = \text{Pa}_{G^*}(x_{j'})$$

$$P_i = \text{Pa}_{G^*}(x_{j'}) \setminus \{x_i\} \quad \text{for } x_i \in \text{Pa}_{G^*}(x_{j'}).$$

We would again like to understand if certain score functions favor incorrect P_i parent sets when the parents have non-linear effects on the target. We call this evaluation procedure the *Correct Parent Deletion* task. These two tasks are illustrated in Fig. 4.

We consider the following benchmark procedures. The first three methods are linear, and use the BIC score (with different estimates of the covariance matrix). In particular, the BIC score for Gaussian errors is a function of the target node x_j , parent set P_j , and estimated covariance matrix $\hat{\Sigma}$:

$$\text{BIC}(x_j, P_j, \hat{\Sigma}) = - \left(\frac{N}{2} \log(2\pi \hat{\sigma}_{j|P_j}^2) + \frac{N}{2} \right) - .5 \log(N)(|P_j| + 2), \quad (11)$$

where the conditional noise variance (based on Schur complements) equals

$$\hat{\sigma}_{j|P_j}^2 = \hat{\Sigma}_{jj} - \hat{\Sigma}_{jP_j} \hat{\Sigma}_{P_j P_j}^{-1} \hat{\Sigma}_{P_j j}.$$

Benchmark Methods.

- (a) **Vanilla BIC:** scores each parent set by inputting the sample covariance matrix $\frac{1}{N} X^T X$ into Eq. (11).
- (b) **LRPS + BIC:** scores each parent using the covariance matrix estimated from a low-rank plus sparse (LRPS) decomposition of the sample precision matrix; see Frot et al. (2019). We use the author’s code in R to fit this decomposition, and pick the hyperparameters using cross-validation.
- (c) **PCSS + BIC:** scores each parent using the covariance matrix $\frac{1}{N}(X - S)^T(X - S)$, where S is the output from Algorithm 1. We pick one principal component and 3 principal components for the linear and non-linear case, respectively. This choice was based on visual inspection of the spectrum of the covariance matrix. See the Appendix.

- (d) **CAM**: scores each parent via Eq. (10) but sets S_{C_j} equal to the zero matrix (i.e., the marginal likelihood from a vanilla Gaussian process CAM model).
- (e) **CAM-OBS**: scores each parent via Eq. (10) but sets S_{C_j} equal to h (the true confounders) and $\tilde{X}_i = X_i$ instead.

For both parent set tasks, we fix $N = 250$ and $p = 500$ but vary the strength of confounding. For the Correct Parent Deletion task, we exclude the linear trend from the set of trends when generating non-linear data to focus on the particular problem of modeling non-linearities as described above. Apart from that, the data in both settings are generated as specified at the beginning of this section. Fig. 5 shows the non-linear SEM results. The remaining results are shown in Fig. D.1 and Fig. D.2. In these figures, the different methods are compared using the following metric:

Prop. Times MLL Wrong > MLL True: out of the M incorrect parent sets, what proportion have scores larger than the true parent set. Lower is better here.

Our findings based on this analysis are: Fig. 5 and Fig. D.1 show that methods that account for confounders (i.e., LRPS+BIC, PCSS+BIC, CAM-OBS, DeCAMFound), place higher probability on the correct parent set for the Wrong Parent Addition task across different settings relative to those that do not model the confounders. In addition, Fig. 5 and Fig. D.2 show that for the Correct Parent Deletion task, as expected, the linear methods suffer in the non-linear setting. Note that unlike PCSS+BIC, LRPS+BIC suffers even in the linear setting because it induces a very sparse graph, causing it to delete true parents. Also note that it is not possible to run CAM-OBS in practice, since it requires knowing the unobserved confounders h ; we include it merely as a benchmark to understand how parent set recovery is affected by estimation error (i.e., only having finite observational data) rather than latent confounding. Interestingly, our method, which does not require knowing h , sometimes outperforms CAM-OBS. This might be because our method leverages all p observed nodes to estimate the confounding variation via PCA. CAM-OBS, on the other hand, estimates the confounding variation one node at a time (i.e., by regressing each observed node on h). Finally, all methods suffer when the confounding strength increases since the observed signal necessarily becomes weaker. We provide additional empirical results including a DAG evaluation scoring task in Appendix D.1.

5.2. Real Data: Ovarian Cancer Dataset

We use the (pre-processed) ovarian cancer RNA-seq dataset from Frot et al. (2019) which consists of $N = 247$ human samples and $p = 501$ genes. There are 15 total transcription factors (TFs), and the remaining 486 genes interact with at least one of these TFs. This dataset has a partial ground truth, namely that the 15 TFs should precede the 486 genes in the true causal ordering. The reference network for the 501 variables is obtained using Netbox, a software tool for performing network analysis using biological knowledge and community network-based approaches (Cerami et al., 2010). A caveat, however, is that edges in this network might not have a precise probabilistic meaning (i.e., in either a causal or undirected probabilistic graphical model sense).

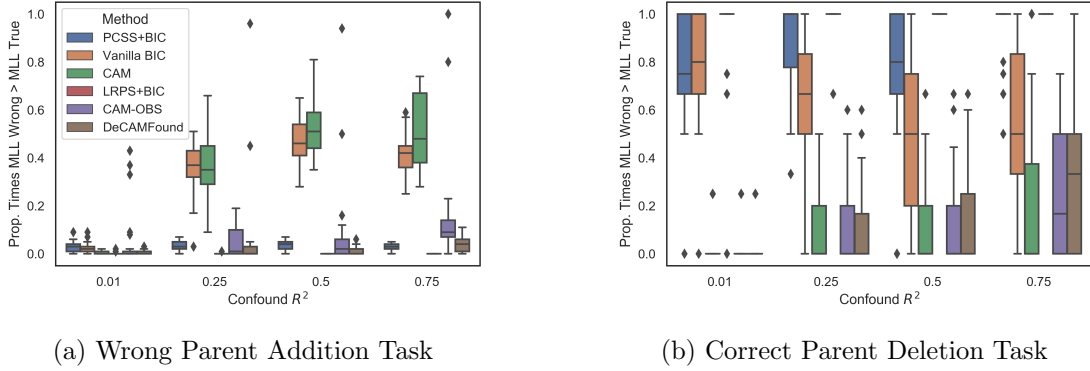


Figure 5: Results for the Wrong Parent Addition and Correct Parent Deletion tasks (lower values on the y-axis are better for both tasks). The data are generated according to a non-linear SEM. 25 total simulations per dataset configuration were performed.

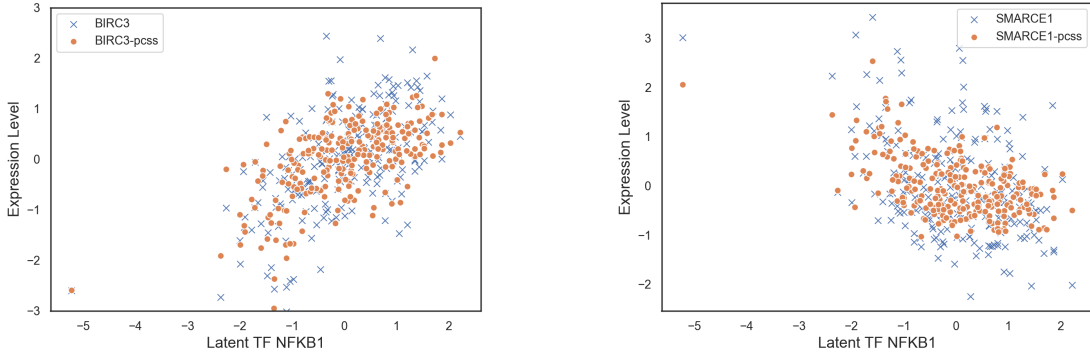


Figure 6: The two genes most positively and negatively correlated with the transcription factor NFKB1, respectively. GENE-pcss refers to the total latent confounding variation estimated for that gene via PCSS. GENE refers to the observed values of the gene.

One way the authors in Frot et al. (2019) benchmarked their methods was by counting the number of directed edges from TFs to genes that agree with the edges in NetBox. The authors stated that confounding can be expected in this dataset due to unobserved transcription factors or batch effects. We here take a different approach for the evaluation and instead *explicitly* create confounders by design. In particular, we remove all 15 TFs from the dataset and assume that we only observed the remaining 486 genes.

5.2.1. Estimating the Confounding Variation

By removing the TFs, we can evaluate the methods in a similar fashion as the simulated experiments since we know the true values of the TFs. In the following, we first assess our ability to estimate s . Suppose that an observed gene x_j is strongly correlated with one of the 15 latent TFs t_k . Then, we would expect that $\mathbb{E}[x_j^{(n)} | t_k = t_k^{(n)}] \approx \mathbb{E}[x_j^{(n)} |$

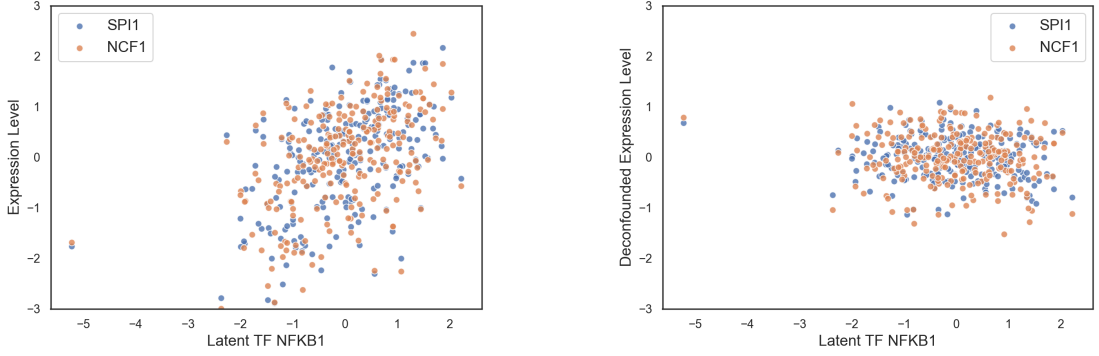


Figure 7: Both genes have a correlation greater than 0.4 with NFKB1 (left hand plot). After subtracting out the confounding variation estimated using PCSS for each gene (denoted as “deconfounded” expression level), the genes are no longer correlated with the unobserved transcription factor NFKB1.

$h = h^{(n)}] = s_j^{(n)}$. Since we know t_k , we can produce a similar plot as in Fig. 3. To this end, we look at NFKB1 which is a TF known to be associated with ovarian cancer (Harrington and Annunziata, 2019). In Fig. 6, we look at the highest positive and negatively correlated genes with NFKB1, which are BIRC3 and SMARCE1 respectively. We see that the estimated confounding variation for each gene estimated from PCSS correlates well with the unobserved TF NFKB1. This suggests that the confounding variation estimated from PCSS corresponds to true confounding (i.e., in this instance NFKB1).

5.2.2. Parent Recovery Performance

Unlike in the simulated dataset experiments, we do not know the true causal graph. In Frot et al. (2019), the authors used the graph structure predicted by NetBox as one way to evaluate their methods. We follow a similar strategy in order to replicate the parent evaluation tasks from the simulated data experiments. We do this by first treating the graph outputted by NetBox as the ground truth undirected graph. Since we do not know the true parent sets for each node, we use the neighborhood set in the undirected graph as a proxy. Hence, to find genes likely to have spurious edges due to the removed TFs, we consider the set of gene pairs that are conditionally independent given the TFs and neighborhood sets of each node but marginally dependent given just the neighborhood sets. For each ordered pair of genes, we select the first element to be the target node and the second element as the spurious parent to add. We take the neighborhood set of the target nodes as the proxy for the true parent set, and score this neighborhood set relative to the neighborhood set appended with the wrong parent candidate. For each method, we compute the proportion of times that the neighborhood set appended with the wrong parent candidate has a higher score than just the neighborhood set (i.e., analogous to the Wrong Parent Addition task). Since the 15 removed TFs have high node degrees, many gene pairs satisfy the criteria above (which would require us to score

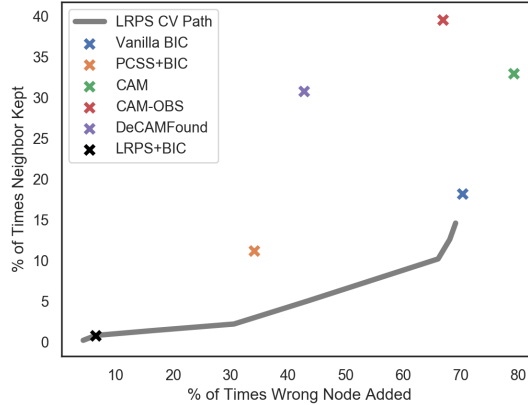


Figure 8: The x-axis denotes the proportion of times a method scored the incorrect parent appended to the neighborhood set higher than just the neighborhood set of a node (i.e., our proxy for the true parent set). The y-axis denotes the proportion of times a method scored the full neighborhood set higher than the neighborhood set after removing out one of the neighbors. For LRPS, we provide the intermediate results for each covariance matrix outputted along its cross-validation path. The black ‘x’ for LRPS corresponds to the performance of the covariance matrix selected based on cross-validation. We compute the *positive likelihood ratio* for each method which equals the ratio between our proxy for the true positive rate (i.e., the y-axis) and false positive rate (i.e., the x-axis). These ratios are as follows: Vanilla BIC=.26, PCSS+BIC=.33, CAM=.42, CAM-OBS=.59, DeCAMFound= .72, LRPS+BIC=.12.

about 70K possible parent sets). Instead, we focus on a subset of edges with at least one strong TF confounder. In particular, we require that each node in the formed edge have correlation greater than 0.4 with one of the 15 removed TFs. This choice makes it more likely that one of the 15 left out TFs is the actual confounder rather than e.g., batch effects, and results in roughly 1000 parent sets to score. One such gene pair with a strong TF confounder is illustrated in Fig. 7. We see how removing the confounder sufficient statistics from each gene results in removing the shared confounding effect of the strongest transcription factor NFKB1.

To also evaluate a method’s statistical power / ability to detect edges, we randomly sample 500 edges from the NetBox undirected graph. For each edge, we randomly select one of the edges as the target node and consider removing the second node from the target node’s neighborhood set. In particular, we check if a method scores the parent set with the second node removed from the neighborhood set lower than the full neighborhood set (i.e., similar to the Correct Parent Deletion task).

The results for both tasks are summarized in Fig. 8. We see that LRPS produces a very sparse graph, and hence almost never adds a wrong parent. However, it almost always removes true edges, which comes at the expense of statistical power. Our method has the highest power per unit of false positives. Rather surprisingly, CAM-OBS, which explicitly uses the 15 held out transcription factors, selects wrong parents more often

than our method. This might be the result of having additional (pervasive) confounders beyond the 15 TFs we introduced by design, as raised by Frot et al. (2019).

6. Conclusion

In this paper, we showed that we can identify the causal graph G^* among the observed nodes in the setting of non-linear effects and pervasive confounders. We proposed a practical algorithm, the DeCAMFounder, to consistently estimate G^* using Gaussian processes. Since the DeCAMFounder explicitly accounts for confounders and non-linear effects, we found improved performance on both simulated and real datasets relative to existing methods.

There are a number of interesting future directions. One involves improving scalability; our current method takes $O(N^3)$ time to score a single parent set since we must invert an $N \times N$ kernel matrix. An interesting direction is to improve computation time by making use of existing techniques for large-scale kernel matrix approximation; see, for example, Titsias (2009); Drineas and Mahoney (2005); Agrawal et al. (2019). Another interesting direction is to explore how to handle selection bias. In Frot et al. (2019), for example, the authors showed how to account for selection bias and pervasive confounders in the linear setting. It would be interesting to explore whether a similar idea could be used to extend the DeCAMFounder to handle selection bias.

Acknowledgements. The authors were partially supported by NSF (DMS-1651995), ONR (N00014-17-1-2147 and N00014-18-1-2765), IBM, and a Simons Investigator Award to C. Uhler. In addition, C. Squires was partially supported by an NSF Graduate Fellowship (Grant No. 1745302).

References

- Agrawal, R., Campbell, T., Huggins, J. and Broderick, T. (2019) Data-dependent compression of random features for large-scale kernel approximation. *International Conference on Artificial Intelligence and Statistics*.
- Bernstein, D., Saeed, B., Squires, C. and Uhler, C. (2020) Ordering-based causal structure learning in the presence of latent variables. *Proceedings of Machine Learning Research*, **108**, 4098–4108.
- Bühlmann, P., Peters, J. and Ernest, J. (2014) CAM: Causal additive models, high-dimensional order search and penalized regression. *Annals of Statistics*, **42**, 2526–2556.
- Cai, J.-F., Candès, E. J. and Shen, Z. (2010) A singular value thresholding algorithm for matrix completion. *SIAM Journal on Optimization*, **20**, 1956–1982.
- Cerami, E., Demir, E., Schultz, N., Taylor, B. S. and Sander, C. (2010) Automated network analysis identifies core pathways in glioblastoma. *PLOS ONE*, **5**, 1–10.
- Chandrasekaran, V., Parrilo, P. A. and Willsky, A. S. (2012) Latent variable graphical model selection via convex optimization. *Annals of Statistics*, **40**, 1935–1967.

- Chandrasekaran, V., Sanghavi, S., Parrilo, P. A. and Willsky, A. S. (2009) Sparse and low-rank matrix decompositions. In *2009 47th Annual Allerton Conference on Communication, Control, and Computing (Allerton)*, 962–967.
- Chickering, D. M. (2002) Optimal structure identification with greedy search. *Journal of Machine Learning Research*, **3**, 507–554.
- Colombo, D., Maathuis, M. H., Kalisch, M. and Richardson, T. S. (2012) Learning high-dimensional directed acyclic graphs with latent and selection variables. *Annals of Statistics*, **40**, 294–321.
- Davis, C. and Kahan, W. (1970) The rotation of eigenvectors by a perturbation III. *SIAM J. Numer. Anal.*, **7**, 1–46.
- Drineas, P. and Mahoney, M. (2005) On the Nyström method for approximating a Gram matrix for improved kernel-based learning. *Journal of Machine Learning Research*, 2153–2175.
- Fan, J., Liao, Y. and Mincheva, M. (2013) Large covariance estimation by thresholding principal orthogonal complements. *Journal of the Royal Statistical Society Series B*, **75**, 603–680.
- Friedman, N., Linial, M., Nachman, I. and Pe’er, D. (2000) Using Bayesian networks to analyze expression data. In *Proceedings of the Fourth Annual International Conference on Computational Molecular Biology*, 127–135.
- Friedman, N. and Nachman, I. (2000) Gaussian process networks. In *Proceedings of the 16th Conference on Uncertainty in Artificial Intelligence*, 211–219.
- Frot, B., Nandy, P. and Maathuis, M. H. (2019) Robust causal structure learning with some hidden variables. *Journal of the Royal Statistical Society: Series B*, **81**, 459–487.
- Gardner, J., Pleiss, G., Weinberger, K. Q., Bindel, D. and Wilson, A. G. (2018) GPyTorch: Blackbox matrix-matrix Gaussian process inference with GPU acceleration. In *Advances in Neural Information Processing Systems*.
- Gyorfi, L., Kohler, M., Krzyzak, A. K. and Walk, H. (2003) A distribution-free theory of nonparametric regression. *Journal of the American Statistical Association*, **98**, 1084–1084.
- Harrington, B. S. and Annunziata, C. M. (2019) NF- κ B signaling in ovarian cancer. *Cancers (Basel)*, **8**.
- Hauser, A. and Bühlmann, P. (2012) Characterization and greedy learning of interventional Markov equivalence classes of directed acyclic graphs. *Journal of Machine Learning Research*, **13**, 2409–2464.
- Hoyer, P., Janzing, D., Mooij, J. M., Peters, J. and Schölkopf, B. (2009) Nonlinear causal discovery with additive noise models. In *Advances in Neural Information Processing Systems*, vol. 21.

- Kalisch, M. and Bühlmann, P. (2007) Estimating high-dimensional directed acyclic graphs with the PC-algorithm. *Journal of Machine Learning Research*, **8**, 613–636.
- Kusner, M. J., Loftus, J., Russell, C. and Silva, R. (2017) Counterfactual fairness. In *Advances in Neural Information Processing Systems*, vol. 30.
- Leek, J. T. and Storey, J. D. (2007) Capturing heterogeneity in gene expression studies by surrogate variable analysis. *PLOS Genetics*, **3**.
- Mooij, J. M., Janzing, D., Peters, J. and Schölkopf, B. (2009) Regression by dependence minimization and its application to causal inference in additive noise models. In *Proceedings of the 26th Annual International Conference on Machine Learning, ICML 2009, Montreal, Quebec, Canada, June 14-18, 2009*, vol. 382, 745–752.
- Mooij, J. M., Peters, J., Janzing, D., Zscheischler, J. and Schölkopf, B. (2016) Distinguishing cause from effect using observational data: Methods and benchmarks. *Journal of Machine Learning Research*, **17**, 1–102.
- Pearl, J. (2009) *Causality: Models, Reasoning and Inference*. Cambridge University Press, 2nd edn.
- Peters, J., Mooij, J. M., Janzing, D. and Schölkopf, B. (2014) Causal discovery with continuous additive noise models. *Journal of Machine Learning Research*, **15**, 2009–2053.
- Price, A., Patterson, N., Plenge, R., Weinblatt, M., Shadick, N. and Reich, D. (2006) Principal components analysis corrects for stratification in genome-wide association studies. *Nature Genetics*.
- Rasmussen, C. E. and Williams, C. K. I. (2006) *Gaussian Processes for Machine Learning*. The MIT Press.
- Richardson, T. and Spirtes, P. (2002) Ancestral graph markov models. *Annals of Statistics*, **30**, 962–1030.
- Robins, J., Hernan, M. A. and Brumback, B. (2000) Marginal structural models and causal inference in epidemiology. *Epidemiology*, **11**, 550–60.
- Rudin, W. (1974) *Functional Analysis*. International series in pure and applied mathematics. Tata McGraw-Hill.
- Shah, R. D., Frot, B., Thanei, G.-A. and Meinshausen, N. (2020) Right singular vector projection graphs: fast high dimensional covariance matrix estimation under latent confounding. *Journal of the Royal Statistical Society: Series B (Statistical Methodology)*, **82**, 361–389.
- Solus, L., Wang, Y., Matejovicova, L. and Uhler, C. (2020) Consistency guarantees for permutation-based causal inference algorithms. *Biometrika*, asaa104.
- Spirtes, P., Glymour, C. and Scheines, R. (2000) *Causation, Prediction, and Search*. The MIT Press, 2nd edn.

- Titsias, M. K. (2009) Variational learning of inducing variables in sparse Gaussian processes. In *International Conference on Artificial Intelligence and Statistics*.
- Wang, W. and Fan, J. (2017) Asymptotics of empirical eigenstructure for high dimensional spiked covariance. *Annals of Statistics*, **45**, 1342–1374.
- Wang, Y. and Blei, D. M. (2019) The blessings of multiple causes. *Journal of the American Statistical Association*, **114**, 1574–1596.

A. Proofs

A.1. Proof of Proposition 1

Proof. Let $O = \{x_1, \dots, x_p\}$ and $\mathbb{P}(x, h)$ be Markov with respect to a DAG G . Then, there exist functions g_j and f_j such that

$$\begin{aligned} h_i &= g_i(\text{Pa}_G(h_i), h'_i) \quad \forall i \in [K] \\ x_j &= f_j(\text{Pa}_G(x_j), \epsilon_j) \quad \forall j \in [p], \end{aligned} \quad (12)$$

where the noises $h' \perp\!\!\!\perp \epsilon$. We prove the claim by inducting on the number of confounders K . For $K = 1$, $\text{Pa}_G(h_1) \subset O$. Hence, h_1 is only a function of h'_1 and the observed nodes. Consider the graph G' formed by removing node h_1 (and all corresponding incoming and outgoing arrows) in G and adding a new node h'_1 . Let $\text{Pa}_{G'}(h'_1) = \emptyset$ and $\text{Ch}_{G'}(h'_1) = \text{Ch}_G(h_1)$, where $\text{Ch}_G(h)$ denotes the children of node h in the graph G . For every $x_i \in \text{Ch}_G(h_1)$, add $\text{Pa}_G(h_1)$ to the parent set of x_i in G' . Then, G' is a DAG and h' is a source. Furthermore, the partial order induced by G' equals the partial order induced by G on the subset of observed nodes $\{x_1, \dots, x_p\}$. It suffices to show that $\mathbb{P}(x, h')$ is Markov with respect to G' . Then, for any $x_j \in \text{Ch}_{G'}(h')$,

$$\begin{aligned} x_j &= f_j(\text{Pa}_G(x_j) \setminus h_1, h_1, \epsilon_j) \\ &= f_j(\text{Pa}_G(x_j) \setminus h_1, g_1(\text{Pa}_G(h_1), h'_1), \epsilon_j). \end{aligned} \quad (13)$$

Hence, x_j functionally only depends on the parent set specified by G' . Since the parent sets of G' agree with G on the remaining set of observed nodes, the claim holds for $K = 1$.

Assume that for any set of p observed nodes and $K - 1$ confounders, we can always construct such a DAG G' . Suppose that there are K total confounders. Without loss of generality, suppose that $\text{Pa}_G(h_1) \subset O$ (i.e., h_1 comes before h_2, \dots, h_K in the causal ordering). Treat $x_1, \dots, x_p, h_2, \dots, h_K$ as the set of observed nodes. Then, h_1 is the only confounder. Hence, by the inductive hypothesis, there exists a DAG G' and exogenous h'_1 such that $x_1, \dots, x_p, h'_1, h_2, \dots, h_K$ factorizes according to G' . To complete the proof, treat x_1, \dots, x_p, h'_1 as the set of observed nodes, and h_2, \dots, h_K as the set of confounders. Then, there are $K - 1$ total confounders. Applying the inductive hypothesis again, there exists a DAG G'' such that $x_1, \dots, x_p, h'_1, h''_2, \dots, h''_K$ factorizes according to G'' and h''_2, \dots, h''_K are sources. Since we picked h_1 to come before h_2, \dots, h_p in the causal ordering in G , h'_1 remains a source in G'' . Hence, $h'_1, h''_2, \dots, h''_K$ are all sources as desired. \square

A.2. Proof of Lemma 1

Proof. By Eq. (2),

$$x = (I - B)^{-1}\epsilon + (I - B)^{-1}\Theta h. \quad (14)$$

Hence,

$$\begin{aligned} x_j &= \sum_{x_i \in \text{Pa}_{G^*}(x_j)} B_{ij}x_i + \Theta_i^T h \\ &= \sum_{x_i \in \text{Pa}_{G^*}(x_j)} B_{ij}[(I - B)^{-1}\epsilon + (I - B)^{-1}\Theta h]_i + \Theta_j^T h. \end{aligned} \quad (15)$$

Taking expectations with respect to h gives

$$\begin{aligned}
s_j &= \mathbb{E}[x_j \mid h] \\
&= \mathbb{E} \left[\sum_{i \in \text{Pa}_{G^*}(x_j)} B_{ij} [(I - B)^{-1} \epsilon + (I - B)^{-1} \Theta h]_i + \Theta_j^T h \mid h \right] \\
&= \sum_{i \in \text{Pa}_{G^*}(x_j)} \mathbb{E} [B_{ij} [(I - B)^{-1} \epsilon + (I - B)^{-1} \Theta h]_i \mid h] + \Theta_j^T h \\
&= \sum_{i \in \text{Pa}_{G^*}(x_j)} [(I - B)^{-1} \Theta h]_i + \Theta_j^T h \quad (\text{since } \epsilon \perp\!\!\!\perp h),
\end{aligned} \tag{16}$$

which completes the proof. \square

A.3. Proof of Theorem 1

Lemma 2. For every $j \in [p]$, there exists an f_j such that

$$x_j = \epsilon_j + d_j + f_j(\epsilon_1, d_1, \dots, \epsilon_{j-1}, d_{j-1}) \tag{17}$$

for the SEM in Eq. (1).

Proof. The proof follows by inducting on the number of nodes in G^* . For $p = 1$, $x_1 = d_1 + \epsilon$, and Eq. (17) trivially holds. For $p = 2$,

$$\begin{aligned}
x_2 &= d_2 + \epsilon_2 + f_{12}(x_1) \\
&= d_2 + \epsilon_2 + f_{12}(d_1 + \epsilon_1).
\end{aligned} \tag{18}$$

The claim holds by setting $f_2(\epsilon_1, d_1) = f_{12}(d_1 + \epsilon_1)$. Suppose that Eq. (17) holds for all DAGs with at most $p - 1$ nodes. Then it suffices to prove that Eq. (17) holds for all DAGs with p nodes. For this, note that

$$\begin{aligned}
x_p &= d_p + \epsilon_p + \sum_{x_i \in \text{Pa}_{G^*}(x_p)} f_{ij}(x_i) \\
&= d_p + \epsilon_p + \sum_{x_i \in \text{Pa}_{G^*}(x_p)} f_{ij}(\epsilon_i + d_i + f_j(\epsilon_1, d_1, \dots, \epsilon_{i-1}, d_{i-1})),
\end{aligned} \tag{19}$$

where the last line follows from the inductive hypothesis. Thus by setting

$$f_p(\epsilon_1, d_1, \dots, \epsilon_{j-1}, d_{j-1}) = \sum_{x_i \in \text{Pa}_{G^*}(x_p)} f_{ij}(\epsilon_i + d_i + f_j(\epsilon_1, d_1, \dots, \epsilon_{i-1}, d_{i-1})),$$

the claim follows. \square

Corollary 3. For an SEM in the form of Eq. (1), it holds that

$$\mathbb{E}[x_j \mid h] = \mathbb{E}[x_j \mid d_1, \dots, d_j].$$

We prove Theorem 1 below using Corollary 3.

Proof. By Eq. (1), it suffices to show that there exists an r_j such that $d_j = s_j - r_j(s_1, \dots, s_{j-1})$ for every $j \in [p]$. We prove this claim by inducting on the number of nodes in G^* . For $p = 1$, $x_1 = d_1 + \epsilon_1$. Since $h \perp\!\!\!\perp \epsilon$, $s_1 = d_1$, and the claim holds by setting $r_1 = 0$. For $p = 2$, $x_2 = \epsilon_2 + d_2 + f_{12}(x_1)$, where f_{12} may equal 0 if x_1 is not a parent of x_2 . Then,

$$\begin{aligned}
s_2 &= \mathbb{E}[x_2 \mid h] \\
&= \mathbb{E}[x_2 \mid d_1, d_2] \quad (\text{by Corollary 3}) \\
&= \mathbb{E}[d_2 + \epsilon_2 + f_{12}(x_1) \mid d_1, d_2] \\
&= d_2 + \mathbb{E}[f_{12}(x_1) \mid d_1] \\
&= d_2 + \mathbb{E}[f_{12}(x_1) \mid s_1] \quad (\text{since } s_1 = d_1).
\end{aligned} \tag{20}$$

Hence, $d_2 = s_2 - \mathbb{E}[f_{12}(x_1) \mid s_1]$. The claim holds by setting $r_2(s_1) = \mathbb{E}[f_{12}(x_1) \mid s_1]$. Suppose that $d_j = s_j - r_j(s_1, \dots, s_{j-1})$ for all SEMs in the form of Eq. (1) with at most $p-1$ nodes. It suffices to show that there exists an r_p such that $d_p = s_p - r_p(s_1, \dots, s_{p-1})$ for an arbitrary SEM in the form of Eq. (1) with p nodes.

For this, consider the subgraph formed from x_1, \dots, x_{p-1} . Since x_p is a sink node, $\mathbb{P}(x_1, \dots, x_{p-1})$ factorizes according to a DAG. Hence, by the inductive hypothesis, there exists $\{r_j\}_{j=1}^{p-1}$ such that

$$d_j = s_j - r_j(s_1, \dots, s_{j-1}) \quad \forall j = 1, \dots, p-1. \tag{21}$$

Now, note that

$$\begin{aligned}
s_p &= \mathbb{E}[x_p \mid h] \\
&= \mathbb{E}[x_p \mid d_1, d_2, \dots, d_p] \quad (\text{by Corollary 3}) \\
&= \mathbb{E}[d_p + \epsilon_p + \sum_{x_i \in \text{Pa}_{G^*}(x_p)} f_{ij}(x_i) \mid d_1, d_2, \dots, d_p] \\
&= d_p + \mathbb{E}\left[\sum_{x_i \in \text{Pa}_{G^*}(x_p)} f_{ij}(x_i) \mid d_1, d_2, \dots, d_{p-1}\right] \\
&= d_p + \mathbb{E}\left[\sum_{x_i \in \text{Pa}_{G^*}(x_p)} f_{ij}(x_i) \mid \{s_i - r_i(s_1, \dots, s_{i-1})\}_{i=1}^{p-1}\right] \quad (\text{by Eq. (21)}).
\end{aligned} \tag{22}$$

Thus by setting

$$r_p(s_1, \dots, s_{p-1}) = \mathbb{E}\left[\sum_{x_i \in \text{Pa}_{G^*}(x_p)} f_{ij}(x_i) \mid \{s_i - r_i(s_1, \dots, s_{i-1})\}_{i=1}^{p-1}\right], \tag{23}$$

the result follows. \square

A.4. Proof of Proposition 2

We follow Friedman and Nachman (2000) to compute the marginal likelihood. By Theorem 1, the marginal likelihood decomposes as

$$\begin{aligned}
\mathbb{P}(X | G, S) &= \int \mathbb{P}(X | G, \Omega_G) d\mathbb{P}(\Omega_G) \\
&= \int \prod_{j=1}^p \mathbb{P}(X_j - S_j | X_{\text{Pa}_G(x_j)}, S_{C_j}, \Omega_G) d\mathbb{P}(\Omega_G) \\
&= \int \prod_{j=1}^p \mathbb{P}(X_j - S_j | X_{\text{Pa}_G(x_j)}, S_{C_j}, \{f_{ij}\}_{i \in \text{Pa}_G(x_j)}, r_j) d\mathbb{P}(\{f_{ij}\}_{i \in \text{Pa}_G(x_j)}, r_j) \\
&= \prod_{j=1}^p \int \mathbb{P}(X_j - S_j | X_{\text{Pa}_G(x_j)}, S_{C_j}, \{f_{ij}\}_{i \in \text{Pa}_G(x_j)}, r_j) d\mathbb{P}(\{f_{ij}\}_{i \in \text{Pa}_G(x_j)}, r_j) \\
&= \prod_{j=1}^p \mathbb{P}(X_j - S_j | X_{\text{Pa}_G(x_j)}, S_{C_j}).
\end{aligned}$$

Hence,

$$\log \mathbb{P}(X | G, S) = \sum_{j=1}^p \log \mathbb{P}(X_j - S_j | X_{\text{Pa}_G(x_j)}, S_{C_j}).$$

The proof now follows from Equation 2.30 of Rasmussen and Williams (2006).

B. Score Function Details

In our experiments, we used an RBF kernel for the k_{η_j} and $k_{\theta_{ij}}$. The kernel hyperparameters η_j and θ_{ij} refer to the unknown lengthscales in an RBF kernel. We implemented this model using the Gaussian process package `GPYtorch` (Gardner et al., 2018) to fit the kernel hyperparameters (i.e., by maximizing the log marginal likelihood via gradient ascent). We used a total of 100 iterations using the `Adam` optimizer with a learning rate of 0.01. See the `scores.py` file in the “decamfound” folder on the Github repository for our `python` code.

C. Generating Simulated Data

For node x_j with sampled trend types f_{ij} and g_{kj} and weights θ_{ij} and θ'_{kj} , let

$$O_j = \sum_{i \in \text{Pa}_{G^*}(x_j)} \theta_{ij} f_{ij}(x_i) \quad C_j = \sum_{k=1}^K \theta'_{kj} g_{kj}(h_k)$$

represent the (unnormalized) variation explained by the observed and confounder nodes, respectively. We wish to find normalization constants $c_{\text{par},j}$ and $c_{\text{confound},j}$ such that

$$\text{Cov}(c_{\text{par},j} O_j + c_{\text{confound},j} C_j) = 1 - \sigma_{\text{noise}}^2$$

and

$$\text{Cov}(c_{\text{confound},j}C_j) = \sigma_{\text{confound}}^2.$$

Since it may be difficult to analytically solve for these normalization constants, we find them inductively using a Monte Carlo approach. In particular, suppose we have computed the normalization constants $c_{\text{par},i}$ and $c_{\text{confound},j}$ for $i < j$. Then, we take many Monte Carlo samples (we use 10,000 in the experiments) from the marginal distribution over $h, x_1, x_2, \dots, x_{j-1}$. This allows us to estimate $\text{Cov}(C_j)$ and solve for $c_{\text{confound},j}$. Similarly, we may use these samples to estimate $\text{Cov}(O_j, C_j)$, which along with the value of $c_{\text{confound},j}$ and the estimate of $\text{Var}(C_j)$, allows us to solve for $c_{\text{par},j}$ in the first equation. There are several edge cases depending on if x_j has no observed and/or confounder parents:

- (a) If x_j has no observed or confounder parents (i.e., is a source), then set $c_{\text{par},j} = 0$ and $c_{\text{confound},j} = 0$. Set the noise variance for x_j equal to 1.
- (b) If x_j has no confounder parents but at least one observed node parent, then set the signal variance for x_j equal to $\sigma_{\text{signal}}^2 + \sigma_{\text{confound}}^2$.
- (c) If x_j has at least one confounder parents but no observed node parents, then set the noise variance for x_j equal to $\sigma_{\text{noise}}^2 + \sigma_{\text{signal}}^2$.

See the `generate_synthetic_data.py` file in our Github repository for the code.

D. Additional Figures and Experiments

D.1. Synthetic Data Experiments

In Section 5, we reported on the proportion of times the incorrect parent set was selected over the true parent set. We report on the following additional metric to understand how confidently wrong (or correct) each method is:

- (a) **Log Odds (Wrong vs. True):** each score equals the log marginal likelihood (technically an approximation for BIC) of the parent set. Assuming a uniform prior over the set of all parent sets, the log odds (LO) between the wrong and true parent set reduces into the difference between scores:

$$\begin{aligned} \text{LO}_i &= \log \frac{\mathbb{P}(X | P_i)\mathbb{P}(P_i)}{\mathbb{P}(X | P_{\text{correct}})\mathbb{P}(P_{\text{correct}})} \\ &= \text{score}(P_i) - \text{score}(P_{\text{correct}}). \end{aligned} \tag{24}$$

We report $\max_{i \in [M]} \text{LO}_i$ for the Wrong Parent Addition task in Fig. D.1 and for the Correct Parent Deletion task in Fig. D.2. A higher value is worse (i.e., it indicates that a method places higher confidence in an incorrect parent set than the true parent set).

Scoring Candidate DAG Results. We score a candidate set of $M = 100$ incorrect DAGs \mathcal{G} , built from randomly adding or deleting edges multiple times, starting from the true DAG (i.e., the natural extension of our two parent set evaluation tasks). Since scoring a single graph takes $O(pN^3)$ for the non-linear methods, we consider fewer settings (i.e., fix the confounding variance to be equal to the signal variance), and only do 10 total simulations instead of 25. These results are shown in Fig. D.3. We report on two metrics:

- (a) **Avg. Posterior SHD:** equals $\sum_{m=1}^M \text{SHD}(G_m, G^*) \mathbb{P}(G | X)$, where SHD denotes the structural hamming distance to the true graph, and $\mathbb{P}(G | X)$ equals the posterior probability of a graph computed from renormalizing the log marginal likelihood scores. Lower is better.
- (b) **SHD Between MAP and True DAG:** reports the SHD from the true DAG for the highest scoring graph (i.e., the maximum a posteriori estimate). Lower is better.

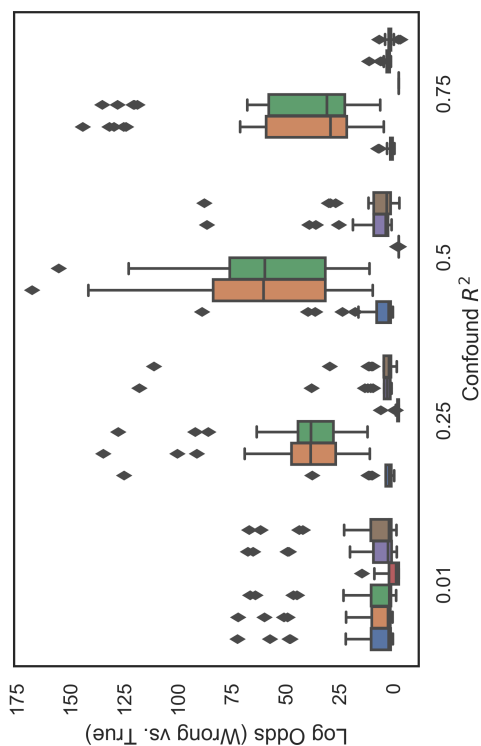
Fig. D.3 shows that linear methods, even if they account for confounding, suffer in the non-linear setting. This advantage of modeling non-linearities agrees with the results, for example, in Bühlmann et al. (2014). Fig. D.3 also shows that, as in the Correct Parent Deletion Task, LRPS suffers even in the linear setting because the induced undirected graph is very sparse (and hence often favors deleting true edges). Finally, Fig. D.3 shows that both CAM-OBS (trivially) and our method are robust to both non-linearities and confounding.

D.2. Ovarian Cancer Dataset

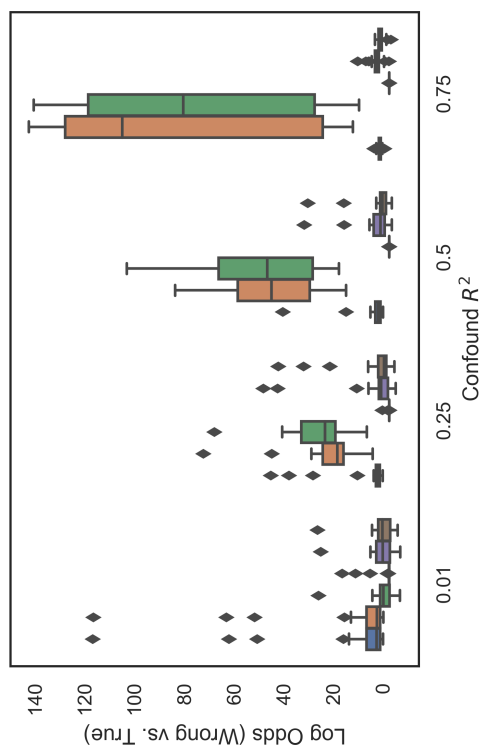
Scree Plot. Analyzing the spectrum of the data matrix consisting of the 486 observed genes in Fig. D.4 shows that there are about 7 spiked eigenvalues.

Pervasive TF Gene Correlations. 7/15 TFs have edges with more than 75 genes according to NetBox (i.e., these TFs might play the role of pervasive confounders). We summarize the absolute value of the correlations between these 7 TFs and the 486 genes in Fig. D.5.

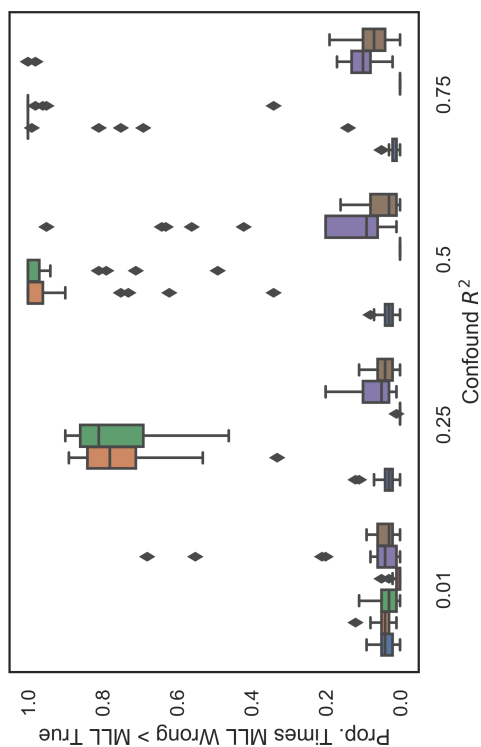
Removing the Effect of a Latent TF via PCSS. See Fig. D.7.



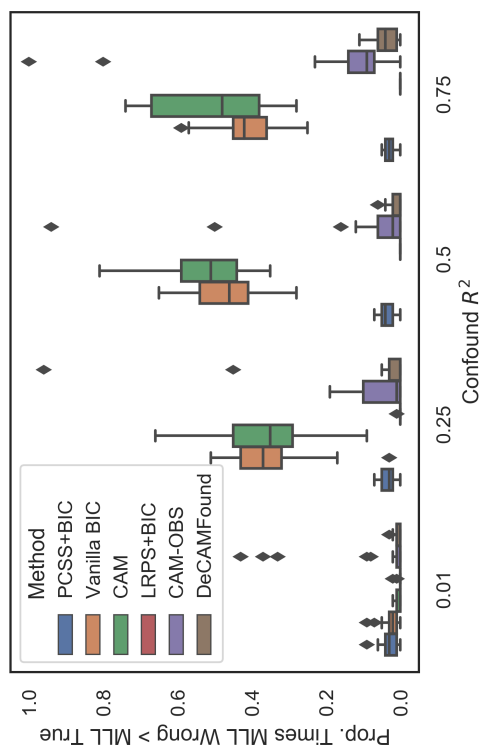
(a) Linear SEM



(b) Linear SEM

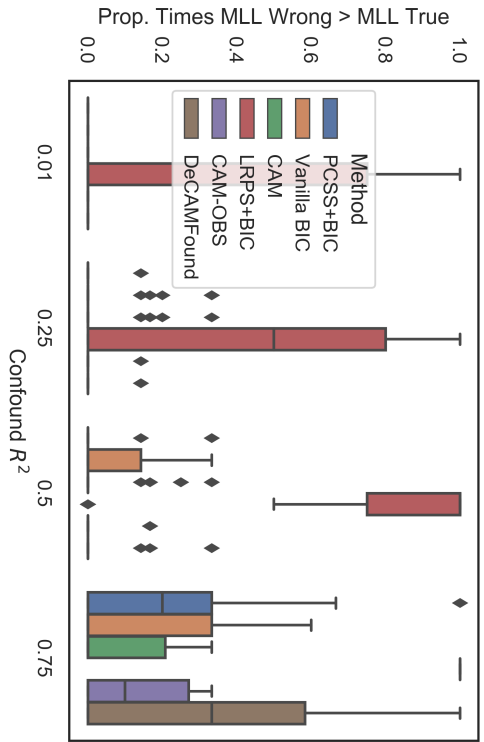


(c) Non-Linear SEM

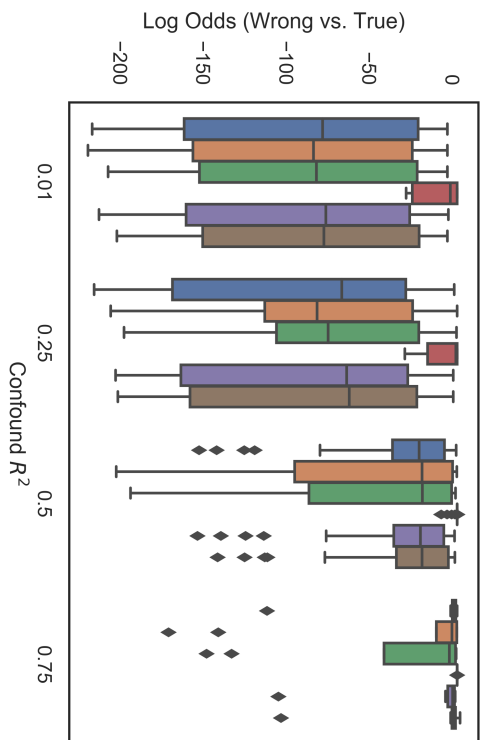


(d) Non-Linear SEM

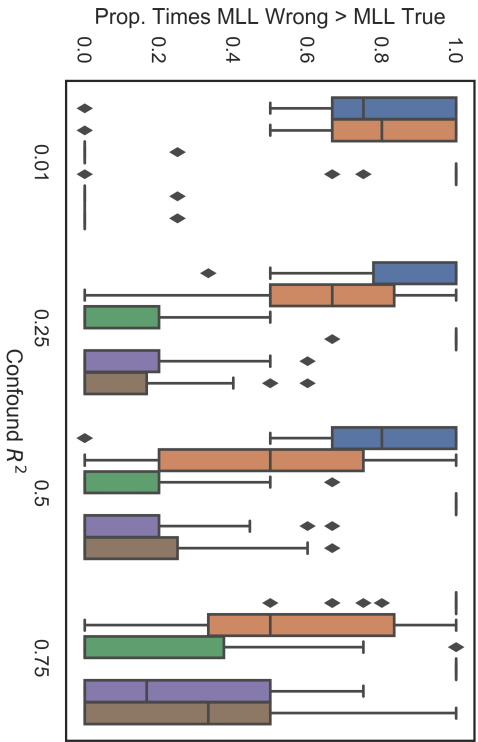
Figure D.1: Results for the Wrong Parent Addition task. 25 total simulations per dataset configuration were performed. See Section 5.1.1.2 and Appendix D.1 for a description of the performance metrics.



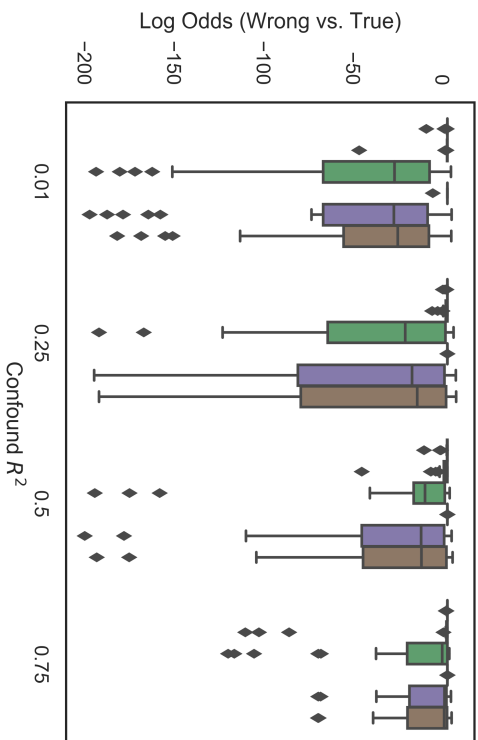
(a) Linear SEM



(b) Linear SEM

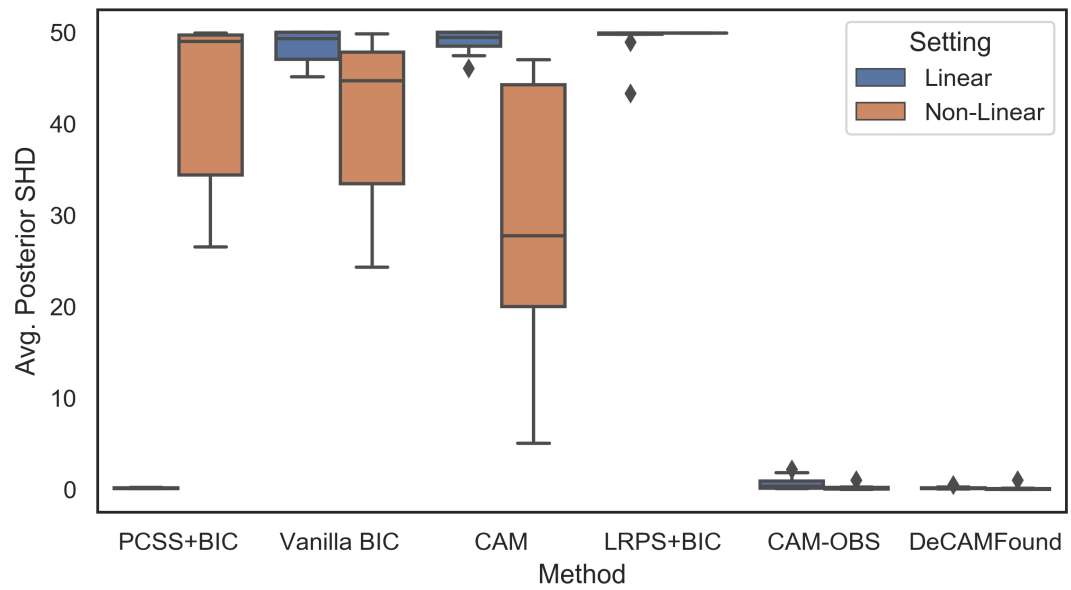


(c) Non-Linear SEM

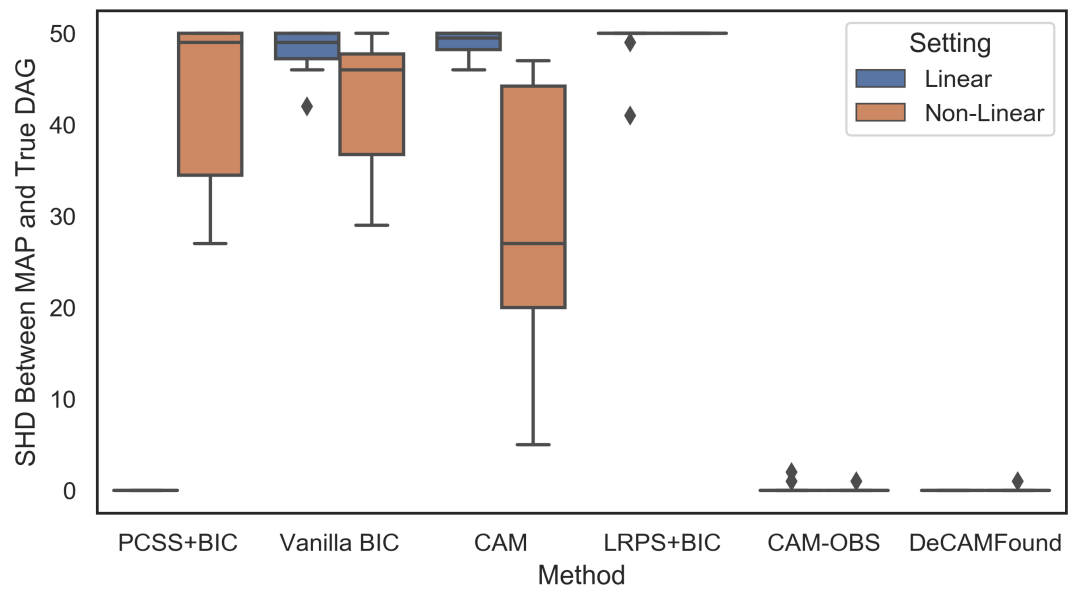


(d) Non-Linear SEM

Figure D.2: Results for the Correct Parent Deletion task. 25 total simulations per dataset configuration were performed. See Section 5.1.2 and Appendix D.1 for a description of the performance metrics.



(a) SHD



(b) Average SHD

Figure D.3: Results for the candidate DAG scoring task. 10 total simulations per dataset configuration (i.e., linear / non-linear) were performed.

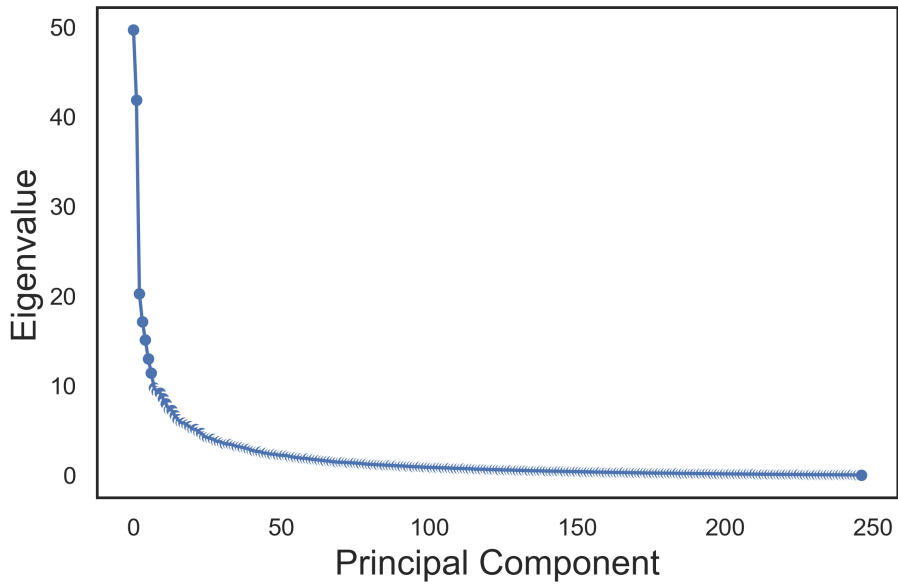


Figure D.4: PCA scree plot when the input data matrix consists of the 486 observed genes. Based on this scree plot, we select $K = 7$ components for the spectral methods.

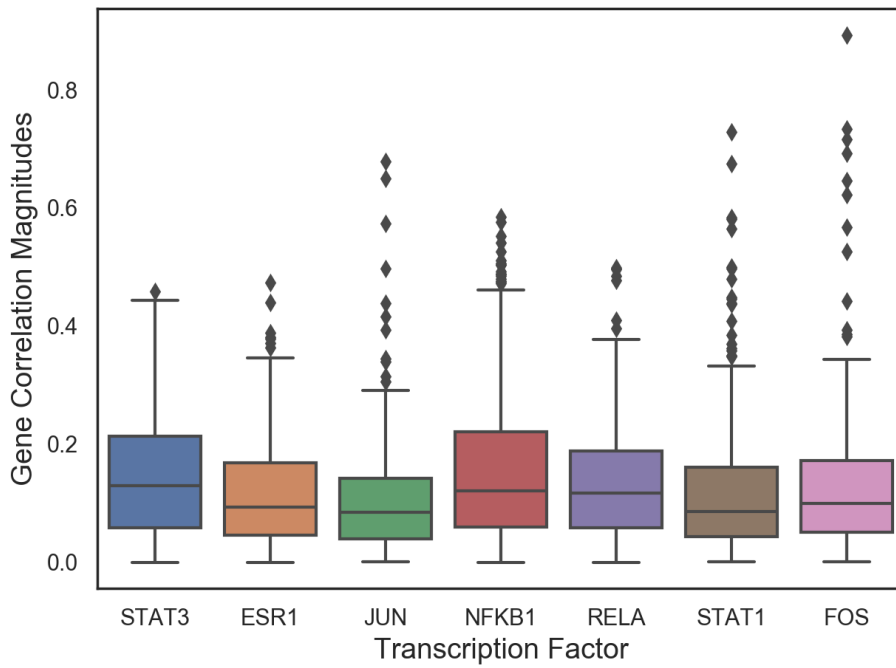


Figure D.5: Absolute value of correlations between TFs and the 486 observed genes. Only TFs with at least 75 edges are shown.

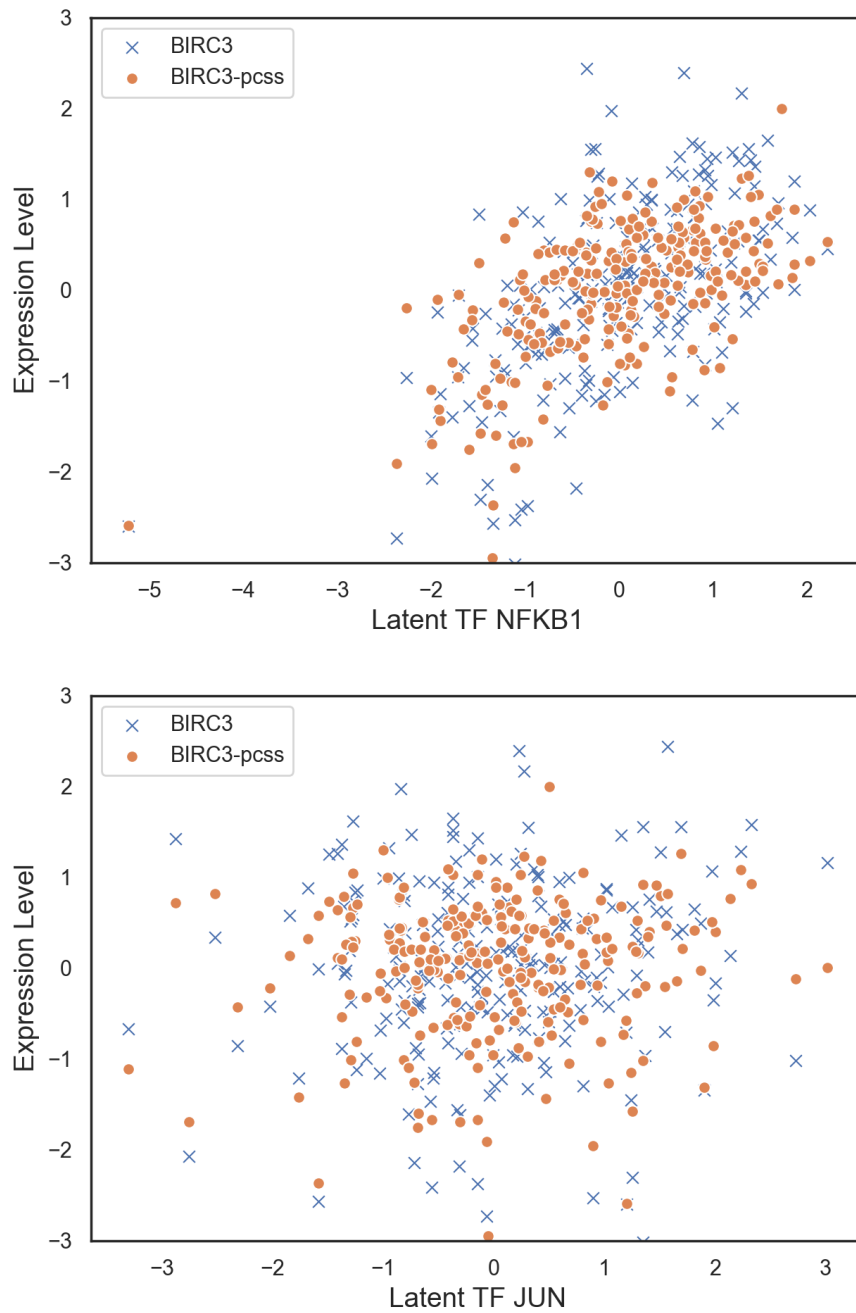


Figure D.6: Out of the 15 latent TFs, BIRC3 has the highest absolute correlation with NFKB1 and the smallest absolute correlation with JUN. BIRC3-pcss refers to the total latent confounding variation estimated for that gene via PCSS. BIRC3 refers to the actual observed values of the gene. BIRC3-pcss is correlated with NFKB1 (which is correlated with BIRC3) and not correlated with JUN.

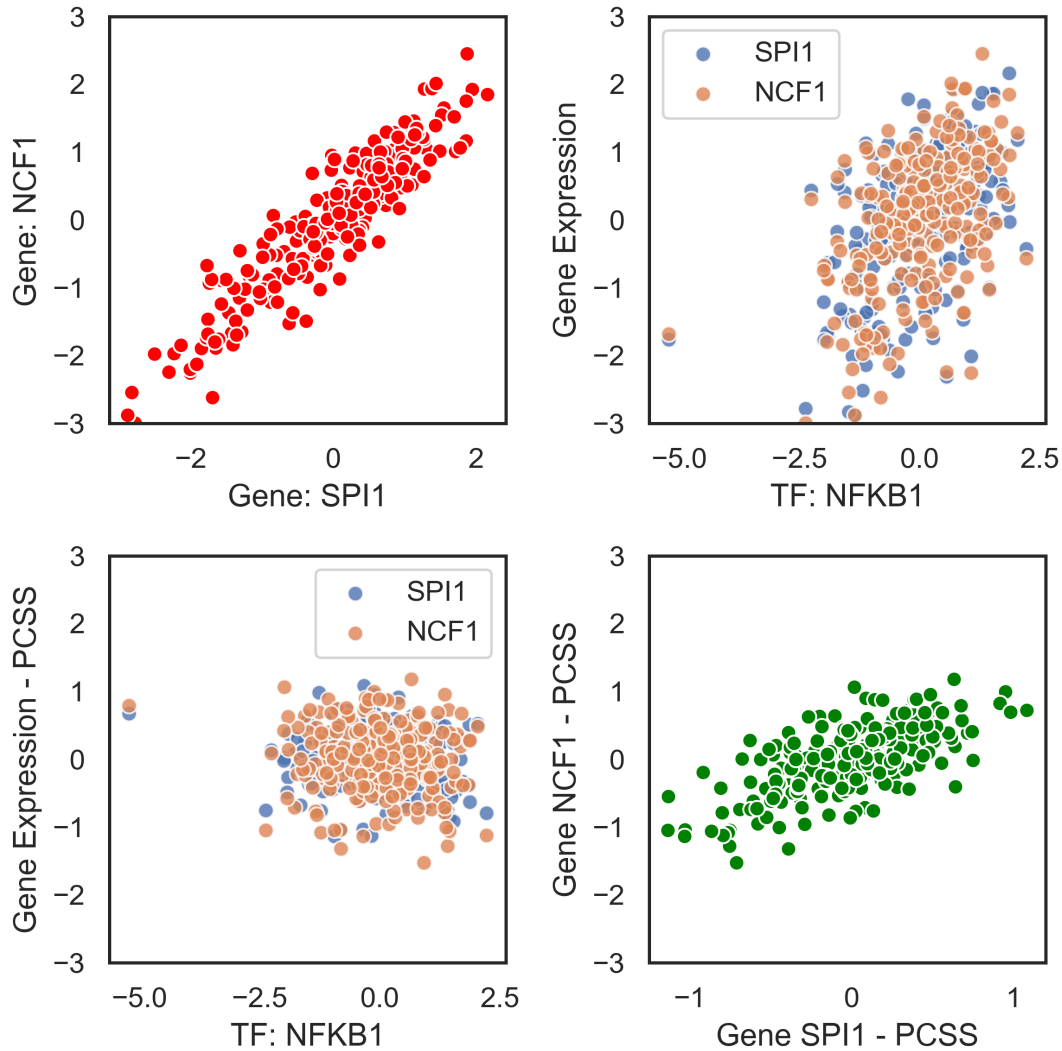


Figure D.7: Top left: scatterplot of two genes that are conditionally independent given each parents' gene neighborhood sets and TFs but dependent when removing the TFs. Top right: scatter plot of each gene for the TF that has the highest correlation with both genes. Bottom left: correlation with the transcription factor after removing the estimated confounder sufficient statistics from each gene. Bottom right: weaker correlation after removing the confounder sufficient statistics from each gene. Since both genes are still marginally dependent given the TFs without conditioning on the parent sets, the genes are still correlated in the bottom right figure.